ESCRT-Dependent Cell Death in a *Caenorhabditis elegans* Model of the Lysosomal Storage Disorder Mucolipidosis Type IV

Julie M. Huynh,* Hope Dang,* Isabel A. Munoz-Tucker,* Marvin O'Ketch,* Ian T. Liu,* Savannah Perno,† Natasha Bhuyan,* Allison Crain,* Ivan Borbon,* and Hanna Fares*,[1]

*Department of Molecular and Cellular Biology, University of Arizona, Tucson, Arizona 85721, and †Sahuaro High School, Tucson, Arizona 85710

ABSTRACT Mutations in *MCOLN1*, which encodes the cation channel protein TRPML1, result in the neurodegenerative lysosomal storage disorder Mucolipidosis type IV. Mucolipidosis type IV patients show lysosomal dysfunction in many tissues and neuronal cell death. The ortholog of TRPML1 in *Caenorhabditis elegans* is CUP-5; loss of CUP-5 results in lysosomal dysfunction in many tissues and death of developing intestinal cells that results in embryonic lethality. We previously showed that a null mutation in the ATP-Binding Cassette transporter MRP-4 rescues the lysosomal defect and embryonic lethality of *cup-5(null)* worms. Here we show that reducing levels of the Endosomal Sorting Complex Required for Transport (ESCRT)-associated proteins DID-2, USP-50, and ALX-1/EGO-2, which mediate the final de-ubiquitination step of integral membrane proteins being sequestered into late endosomes, also almost fully suppresses *cup-5(null)* mutant lysosomal defects and embryonic lethality. Indeed, we show that MRP-4 protein is hypo-ubiquitinated in the absence of CUP-5 and that reducing levels of ESCRT-associated proteins suppresses this hypo-ubiquitination. Thus, increased ESCRT-associated de-ubiquitinating activity mediates the lysosomal defects and corresponding cell death phenotypes in the absence of CUP-5.

KEYWORDS CUP-5; ESCRT; lysosome; mucolipidosis type IV; TRPML1

MUCOLIPIDOSIS type IV (MLIV) is a neurodegenerative lysosomal storage disorder characterized by corneal clouding, achlorhydria, and psychomotor defects (Bach 2001; Altarescu *et al.* 2002). In MLIV patients, large lipid-rich vacuoles are found in many tissues, while psychomotor defects are thought to be due to neuronal cell death. MLIV is caused by mutations in *MCOLN1*, which encodes the human protein mucolipin-1/TRPML1; this protein belongs to the transient receptor potential cation channel family and is a nonselective cation channel (Bargal *et al.* 2000; Bassi *et al.* 2000; Sun *et al.* 2000; Laplante *et al.* 2002; Raychowdhury *et al.* 2004; Dong *et al.* 2008).

Caenorhabditis elegans protein CUP-5 is the ortholog of human TRPML1 (Fares and Greenwald 2001b; Hersh *et al.* 2002). The phenotypes resulting from mutations in *cup-5(null)* mimic those found in MLIV patients: defective lysosomal degradation and the appearance of large vacuoles in most tissues (Fares and Greenwald 2001b; Schaheen *et al.* 2006a). In addition, this lysosomal dysfunction in the absence of CUP-5 leads primarily to the death of developing intestinal cells that results in embryonic lethality (Schaheen *et al.* 2006a). It is not known why developing intestinal cells die in *C. elegans* or why neurons die in MLIV patients. In *C. elegans cup-5(null)* mutants, the embryonic lethality is not solely due to cells undergoing apoptosis from starvation; when ATP levels are restored or when apoptosis is blocked, embryonic lethality is only partially rescued (~14% of embryos hatch and arrest at the L1 larval stage) (Hersh *et al.* 2002; Schaheen *et al.* 2006a).

We have shown that *C. elegans* CUP-5 and mammalian TRPML1 likely function in lysosome formation, which involves the budding of nascent lysosomes from endosomes and scission to release the nascent lysosomes (Treusch *et al.* 2004; Miller *et al.* 2015). In contrast to this outward budding event, Endosomal Sorting Complex Required for

doi: 10.1534/genetics.115.182485
Manuscript received September 3, 2015; accepted for publication November 14, 2015; published Early Online November 19, 2015.
Supporting information is available online at www.genetics.org/lookup/suppl/doi:10.1534/genetics.115.182485/-/DC1.
[1]Corresponding author: University of Arizona, Life Sciences South Bldg., Room 533, 1007 E. Lowell St., Tucson, AZ 85721. E-mail: fares@email.arizona.edu

Transport (ESCRT) proteins are required for the sequestration of integral membrane proteins in intraluminal vesicles through an inward budding and scission event in late endosomes/multivesicular bodies (Henne *et al.* 2011). This ESCRT-dependent targeting of integral membrane proteins includes an early ubiquitination of the cargo and a late de-ubiquitination required for completion of the scission reaction for internalization into an intraluminal vesicle. This de-ubiquitination is carried out by a complex of ESCRT-associated proteins that include Did2p (*Saccharomyces cerevisiae*)/CHMP1b (human), Bro1p (*S. cerevisiae*)/Alix and HD-PTP (human), and Doa4p (*S. cerevisiae*)/USP8 [UBPY] (human) (Bowers *et al.* 2004; Reid *et al.* 2005; Mahul-Mellier *et al.* 2006; Nickerson *et al.* 2006; Richter *et al.* 2007; Row *et al.* 2007; Ali *et al.* 2013). Sequestered cargo is transported to lysosomes for degradation. However, the mechanisms coordinating the sequestration of cargo inside late endosomes and their subsequent transport to lysosomes are unknown.

We have previously shown that mutations in *mrp-4* suppress the *cup-5(null)* lysosomal defect and embryonic lethality (Schaheen *et al.* 2006b). MRP-4 is a member of the ATP-binding cassette (ABC) transporter superfamily found in prokaryotes and eukaryotes that use ATP energy for transport of various molecules across membranes (Bauer *et al.* 1999; Dean *et al.* 2001; Sheps *et al.* 2004). Here, we show that reducing levels of worm ESCRT-associated proteins almost completely suppress the lysosomal defect and embryonic lethality due to the loss of CUP-5. Indeed, we show that, in the absence of CUP-5, misregulated ESCRT-associated protein activity results in altered ubiquitination of MRP-4, which leads to embryonic lethality. Our results implicate ESCRT-associated protein defects in cell death and tissue degeneration in this *C. elegans* model of MLIV.

Materials and Methods

C. elegans strains and methods

Standard methods were used for genetic analysis (Brenner 1974). RNAi was done by the feeding method; control RNAi was done using bacteria expressing the double-stranded RNA generating vector L4440/pPD129.36 (Timmons and Fire 1998). The following markers were used in this study: *arIs37[*P*myo-3*::*ssGFP*; *dpy-20] I* (Fares and Greenwald 2001a); *did-2(ok3325) I* (Moerman and Barstead 2008); *ego-2(om33) I* (Qiao *et al.* 1995; Liu and Maine 2007); *bIs1[vit-2*::*GFP*; *rol-6(su1006)]* (Grant and Hirsh 1999); *unc-36(e251) III* (Brenner 1974); *cup-5(zu223) III* (Hersh *et al.* 2002); *qC1* (Graham and Kimble 1993); *mrp-4(cd8)* (Schaheen *et al.* 2006b); and *pwIs50[lmp-1*::*GFP*, *unc-119(+)]* (Treusch *et al.* 2004). *cup-5(zu223) unc-36(e251)* worms bearing various transgenes were isolated from *qC1*-balanced parent heterozygotes; the eggs from these *cup-5(zu223) unc-36(e251)* homozygous progeny were analyzed in the various assays. The strains used in this study are listed in Table 1.

The following transgenes were made by the bombardment method (Praitis *et al.* 2001): *cdIs146[MRP-4*::*GFP*; *unc-119-ttx-3*::*GFP]*; *cdIs194[LMP-1*:: *LINKER(PGGAGAG GAGAG)*::*TagRFP(S158T)*; *unc-119-ttx-3*::*GFP]*; *cdIs197[DID-2*::*LINKER(PGGAGAGGAGAG)*::*TagRFP(S158T)*; *unc-119-ttx-3*::*GFP]*; *cdIs212[Pelt-2*::*MRP-4*::*LINKER(PGGAGAGGAGAG)*:: *GFP*; *unc-119]*; *cdIs214[DID-2*::*LINKER(PGGAGAGGAGAG)*:: *GFP*; *unc-119]*; *cdIs228[Pelt-2*::*DID-2*; *unc-119]*; *cdIs243[Pelt-2*::*GFP]*; *cdIs262 [Pelt-2*::*MRP-4]*; and *cdEx181[Pelt-2*::*GFP*:: *TagRFP(S158T)*::*RBB-11.1*; *HYGR]*.

Molecular methods

Standard methods were used for the manipulation of recombinant DNA (Sambrook and Russell 2001). PCR was done using the Expand Long Template PCR System (Boehringer Mannheim, Mannheim, Germany), according to the manufacturer's instructions. All other enzymes were from New England Biolabs (Beverly, MA).

Plasmids

Inserts of all plasmids were sequenced to confirm that only the desired changes were introduced. The following plasmids were made and used in this study.

GFP/TagRFP fusion plasmids: The following GFP/TagRFP fusion plasmids were used: pHD233—MRP-4 fused to GFP (S65T) expressed under the control of the *mrp-4* promoter; pHD499—LMP-1 fused to TagRFP(S158T) with an unstructured linker between the two genes and expressed under the control of the *lmp-1* promoter; pHD502—DID-2 fused to TagRFP(S158T) with an unstructured linker between the two genes and expressed under the control of the *did-2* promoter; pHD543—GFP expressed under the control of the *elt-2* promoter; pHD763—*RBB-11.1* fused to TagRFP (S158T) expressed under the control of the *elt-2* promoter; pHD774—DID-2 fused to GFP(S65T) with an unstructured linker between the two genes and expressed under the control of the *did-2* promoter; pHD782—MRP-4 fused to GFP (S65T) with an unstructured linker between the two genes and expressed under the control of the *elt-2* promoter; and pHD823—DID-2 fused to GFP(S65T) expressed under the control of the *elt-2* promoter.

RNAi plasmids used or made with the L4440/pPD129.36 vector: From the Ahringer RNAi library (Kamath and Ahringer 2003) the following were used: *C07G1.5/hgrs-1*, *C09G12.9/tsg-101*, *C27F2.5/vps-22*, *T27F7.1/vps-24*, *Y34D9A.10/vps-4*, *F23C8.6/did-2*, *E01B7.1/usp-50*, *C56C10.3/vps-32.1*, *F21G4.2/mrp-4*, and *W02C12.3/hlh-30*.

From the Orfeome RNAi library (Rual *et al.* 2004) the following were used: *C34G6.7/stam1*, *Y87G2A.10/vps-28*, *ZC64.3/ceh-18*, *W02A11.2/vps-25*, *F17C11.8/vps-36*, *Y46G5A.12/vps-2*, *Y65B4A.3/vps-20*, *F41E6.9/vps-60*, *T24B8.2*, *K10C8.3/istr-1*, and *F37A4.5*.

The following were also used: pHD554, which makes double-stranded RNA corresponding to the last 325 bases

Table 1 *C. elegans* strains used in this study

Name	Genotype
N2	Wild type
GS1912	*dpy-20(e1282); arIs37[Pmyo-3::ssGFP; dpy-20]*
GS2886	*unc-36(e251); bIs1[vit-2::GFP; rol-6(su1006)]*
NP27	*cup-5(zu223) unc-36(e251)/qC1*
NP35	*cup-5(zu223) unc-36(e251)/qC1; arIs37[Pmyo-3::ssGFP; dpy-20]*
NP283	*mrp-4(cd8); cup-5(zu223) unc-36(e251); arIs37[Pmyo-3::ssGFP; dpy-20]*
NP612	*mrp-4(cd8); arIs37[Pmyo-3::ssGFP; dpy-20]*
NP952	*cup-5(zu223) unc-36(e251)/qC1; bIs1[vit-2::GFP; rol-6(su1006)]*
NP1160	*unc-119(ed3); cdIs146[MRP-4::GFP; unc-119-ttx-3::GFP]*
NP1301	*cup-5(zu223) unc-36(e251)/qC1; arIs37; unc-119(ed3); pwIs50[LMP-1::GFP, unc-119]*
NP1332	*unc-119(ed3); cdIs197[DID-2::LINKER::TagRFP(S158T); unc-119-ttx-3::GFP]*
NP1359	*did-2(ok3325); cdIs197[DID-2::LINKER::TagRFP(S158T); unc-119-ttx-3::GFP]*
NP1455	*cup-5(zu223) unc-36(e251)/qC1; unc-75(e950) ego-2(om33) arIs37[Pmyo-3::ssGFP; dpy-20]*
NP1462	*unc-75(e950) ego-2(om33) arIs37[Pmyo-3::ssGFP; dpy-20]*
NP1490	*unc-119(ed3); cdIs214[DID-2::LINKER::GFP; unc-119]*
NP1507	*unc-119(ed3); cdIs212[Pelt-2::MRP-4::LINKER::GFP; unc-119]*
NP1509	*cup-5(zu223) unc-36(e251)/qC1; cdIs214[DID-2::LINKER::GFP; unc-119]*
NP1515	*unc-119(ed3); cdIs197[DID-2::LINKER::TagRFP(S158T); unc-119-ttx-3::GFP]; cdIs212[Pelt-2::MRP-4::LINKER::GFP; unc-119]*
NP1521	*cup-5(zu223) unc-36(e251)/qC1; cdIs212[Pelt-2::MRP-4::LINKER::GFP; unc-119]*
NP1548	*unc-119(ed3); cdIs228[Pelt-2::DID-2; unc-119]*
NP1561	*cup-5(zu223) unc-36(e251)/qC1; cdIs197(DID-2::LINKER::TagRFP(S158T); unc-119-ttx-3::GFP); cdIs212[Pelt-2::MRP-4::LINKER::GFP; unc-119]*
NP1572	*did-2(ok3325)/hT2; cdIs214[DID-2::LINKER::GFP; unc-119]*
NP1591	*cup-5(zu223) unc-36(e251)/qC1; cdIs228[Pelt-2::DID-2; unc-119]*
NP1592	*cup-5(zu223) unc-36(e251)/qC1; cdIs146[MRP-4::GFP; unc-119-ttx-3::GFP]*
NP1597	*unc-119(ed3); cdIs194[LMP-1::TagRFP(S158T); unc-119-ttx-3::GFP]; cdIs212[Pelt-2::MRP-4::LINKER::GFP; unc-119]*
NP1602	*cup-5(zu223) unc-36(e251)/qC1; cdIs194[LMP-1::TagRFP(S158T); unc-119-ttx-3::GFP]; cdIs212[Pelt-2::MRP-4::LINKER::GFP; unc-119]*
NP1684	*cdIs243[Pelt-2::GFP; HYGR]*
NP1687	*cup-5(zu223) unc-36(e251)/qC1; cdIs243[Pelt-2::GFP; HYGR]*
NP1768	*cdIs212[Pelt-2::MRP-4::LINKER::GFP; unc-119]; cdEx181[Pelt-2::GFP::TagRFP(S158T)::RBB-11.1; HYGR]*
NP1779	*cup-5(zu223) unc-36(e251)/qC1; cdIs212[Pelt-2::MRP-4::LINKER::GFP; unc-119]; cdEx181[Pelt-2::GFP::TagRFP(S158T)::RBB-11.1; HYGR]*
NP1789	*cup-5(zu223) unc-36(e251)/qC1; unc-75(e950) ego-2(om33) arIs37[Pmyo-3::ssGFP; dpy-20]; cdIs212[Pelt-2::MRP-4::linkerGFP; unc-119]*
NP1790	*unc-75(e950) ego-2(om33) arIs37[Pmyo-3::ssGFP; dpy-20]; cdIs212[Pelt-2::MRP-4::linkerGFP; unc-119]*
NP1825	*mrp-4(cd8); arIs37; unc-119(ed3); cdIs262[pelt-2::MRP-4 genomic; pmyo-2::GFP; unc-119- Pmyo-2::GFP]*
NP1829	*cup-5(zu223) unc-36(e251)/qC1; mrp-4(cd8); arIs37; cdIs262[pelt-2::MRP-4 genomic;; unc-119- Pmyo-2::GFP]*
RT258	*unc-119(ed3); pwIs50[LMP-1::GFP, unc-119]*

of *did-2* complementary DNA (cDNA); pHD555, which makes double-stranded RNA corresponding to the full 618 bases of *did-2* cDNA; pHD556, which makes double-stranded RNA corresponding to the first 316 bases of *did-2* cDNA; pHD670, which makes double-stranded RNA corresponding to amino acids 710–1154 of *ego-2*; pHD687, which makes double-stranded RNA corresponding to full-length *R10E12.1b/alx-1b* cDNA; pHD758, which makes double-stranded RNA corresponding to amino acids 710–1154 of *ego-2* and full-length cDNA of *alx-1b*; and pHD863, in which MRP-4 is expressed under the control of the *elt-2* promoter.

Plasmid sequences and details on how these plasmids were constructed are available upon request.

Sequence comparison

The DID-2/Did2p/CHMP1b sequence comparison was generated using Clustal Omega (Goujon *et al.* 2010; Sievers *et al.* 2011).

Measuring embryonic viability

Adult worms were allowed to lay eggs overnight on NGM plates at 20° (Brenner 1974). The adults were then removed, and the percentage of eggs that hatched and developed normally was calculated. Each viability measurement consists of at least three experiments and the results show the average of these experiments.

Confocal microscopy

Embryos and adults were placed on a 2.2% agarose pad with 1 mM Levamisole or 9 mM Levamisole, respectively, and images were taken using a Zeiss LSM 510 Meta confocal microscope or a Zeiss 510 Meta confocal microscope, using a 63× lens, an argon 488-nm laser for excitation of the GFP, and a helium neon 543-nm laser for excitation of the RFP. For intensity and compartment size measurements, exposure settings for each assay were set using the wild type or wild-type control RNAi strain and were kept the same for all embryos in the assay. Control worms were always included to ensure that signals did not correspond to autofluorescence or to bleed-through from the other fluorophore. Images were taken of embryos that were between the "comma" and the "1.5-fold" stages of embryonic development because these are the first embryonic stages that show the lysosomal defect in the absence of CUP-5 (Schaheen *et al.* 2006a).

Measurement of intensity and compartment size in embryos

For RNAi experiments, the adult hermaphrodites were placed on the RNAi bacteria, and their laid embryos were analyzed. Measurements of the intensities of GFP and sizes of compartments were done using Metamorph (Sunnyvale, CA) on images that were not modified.

Measurements were made of the sizes and intensities of all VIT-2::GFP-containing compartments within a selected area (213.42 ± 3.28 μm^2) at the base of the intestine. At least 120 discrete intracellular structures from four to eight embryos for each strain and RNAi were used in the measurements.

Pdid-2::*DID*-2::GFP intensity measurements (total, membrane, cytoplasmic) were taken from a selected area (148.19 ± 2.57 μm^2) at the base of the intestine. Twenty to 25 embryos were imaged for each strain. The integrated density (density divided by area) of DID-2::GFP punctate (membrane) and diffuse (cytoplasmic) regions was determined. At least 100 discrete intracellular structures from each strain were used in the measurements. Four randomly chosen diffuse spots were chosen from each area for the DID-2::GFP cytoplasmic measurements.

For P*elt-2*::*DID-2*::*GFP* intensity measurements, 13–14 embryos were imaged for each strain, and the integrated density (density divided by intestine size) was determined for each embryo.

For *Pmrp-4*::*MRP-4*::*GFP* intensity measurements, a z-stack was taken of each embryo (14 embryos imaged for each strain), and the average of the integrated values of all MRP-4::GFP compartments in the intestine from eight layers was determined for each embryo.

For P*elt-2*::*MRP-4*::*GFP* intensity measurements, 20–25 embryos were imaged for each strain, and the average of the integrated values of all MRP-4::GFP compartments in the intestine was determined for each embryo.

For the HLH-30 suppression intensity measurements (*Pdid-2*::*DID*-2::GFP and *Pmrp-4*::*MRP-4*::*GFP*), seven to eight embryos were imaged for each strain, and the average level of each DID-2::GFP/MRP-4::GFP compartment was determined. At least 35 discrete intracellular structures from each strain and RNAi were used in the measurements.

Measurement of lysosomal size and degradation in adults

Hermaphrodites were allowed to lay eggs at 20°. Eggs and worms were collected off the plates in M9 buffer (22 mM KH_2PO_4, 43 mM Na_2HPO_4, 86 mM NaCl, and 1 mM $MgSO_4$) and treated with bleach solution (1% NaClO, 1 M NaOH) to dissolve bacteria and worms and isolate the eggs. The embryos were then washed with M9 buffer and placed on NGM plates lacking OP50 bacteria. The next day, the arrested L1 larvae were transferred to plates with RNAi bacteria, and the worms were imaged when they became adults: *cup-5(zu223) unc-36(e251)* worms were imaged from the *cup-5(zu223) unc-36(e251)/qC1* population. To distinguish between LMP-1::GFP compartments and gut granules found in the intestine, both the argon 488-nm laser for GFP excitation and the helium neon 543-nm laser for RFP excitation were used. The autofluorescent gut granules are excited by both lasers while the LMP-1::GFP compartments are excited only by the argon 488-nm laser. Around four adults were imaged for each strain, and the average level of 10 LMP-1::GFP compartments was determined for each strain. A total of at least 30 discrete LMP-1::GFP compartments was determined from each strain and RNAi.

Immunofluorescence

Embryos laid at 20° and expressing both fusion proteins were fixed on slides for 10 min at −20° with 100% methanol and then for 10 min at −20° with 100% acetone. Samples were then washed twice with PBSTw buffer (1× PBS with 0.1% Tween-20) and then placed in Btw buffer (1× PBS, 1% BSA, 0.1% Tween-20) for 2 hr at 4°. A solution containing primary antibodies diluted in Btw buffer was then added, and the samples were left overnight at 4°. Samples were then washed three times with PBSTw buffer and incubated in a Btw solution containing Cy2- and/or Cy3-labeled secondary antibodies for 2 hr at room temperature in the dark, followed by three washes with PBSTw buffer and imaging. For colocalization studies, the same procedure was performed on embryos expressing only MRP-4::GFP or DID-2::TagRFP as a control for nonspecific binding of antibodies.

Measurement of percentage of colocalization/overlap

The percentage of overlap for MRP::GFP and DID-2::TagRFP in the embryo intestine was calculated using "Just Another Colocalization Plugin" from ImageJ (JACoP; National Institutes of Health, Bethesda, MD) (Schneider *et al.* 2012). The values for the Manders' overlap coefficient M1 were recorded and converted to percentages for the percentage overlap measurement. Eight to 10 embryos were analyzed for each strain.

For measurement of the percentage of colocalization of MRP-4::GFP and LMP-1::TagRFP in the embryo intestine, a z-stack was taken of each embryo (eight to nine embryos for each strain), and the average of the M1 coefficients (calculated by JACoP) from four layers was taken for each embryo. These values were recorded and converted to percentages for the percentage of colocalization.

For measurement of the percentage of colocalization of MRP-4::GFP and LMP-1::TagRFP in the embryo intestine after RNAi of various genes, a z-stack was taken of each embryo (four to seven embryos for each strain and RNAi), and the average of the M1 coefficients (calculated by JACoP) from four layers was taken for each embryo. These values were recorded and converted to percentages for the percentage of colocalization.

For measurement of the percentage of colocalization of MRP-4::GFP and *RBB-11.1*::TagRFP in the embryo intestine, the number of MRP-4::GFP compartments that also had

RBB-11.1::TagRFP were divided by the total number of MRP-4::GFP compartments. Seven to eight embryos were analyzed for each strain.

For measurement of the percentage of colocalization of MRP-4::GFP and *RBB-11.1*::TagRFP in the embryo intestine after RNAi of various genes, the number of MRP-4::GFP compartments that also had *RBB-11.1*::TagRFP were divided by the total number of MRP-4::GFP compartments. Four to eight embryos were analyzed for each strain.

qRT-PCR

Hermaphrodites were allowed to lay eggs at 20°. Eggs and worms were collected off the plates in M9 buffer and treated with bleach solution to dissolve bacteria and worms and isolate the viable eggs. The embryos were then washed three times with M9 buffer and lysed in 0.35 ml of ice-cold Qiagen RNeasy buffer RLT (Qiagen, Germantown, MD) using the Bioruptor Standard sonicator (high power, 15 sec ON/60 sec OFF, eight cycles) (Diagenode, Denville, NJ). Total RNA was isolated using the Qiagen RNeasy kit followed by DNase I digestion (ThermoFisher Scientific, Rockford, IL). RNA concentration was determined using a NanoDrop UV Spectrophotometer (NanoDrop Technologies, Wilmington, DE) before and after DNase 1 digestion. A total of 500 ng of RNA was used to perform oligo(dT) cDNA synthesis with the Power SYBR Green PCR Master Mix (ThermoFisher Scientific). Quantitative PCR was conducted using SYBR Green PCR Master Mix and an ABI 7300 Real Time PCR System (ThermoFisher Scientific). Raw cycle threshold (Ct) values for *mrp-4* were normalized to *elt-2*. Fold changes were calculated using standard ΔCt methods (Pfaffl 2001). Primers for *mrp-4* and *elt-2* were designed to span exon/exon junctions to further reduce the chances of genomic DNA amplification. The following primers were used for qRT-PCR: *mrp-4* forward and reverse—GACCATTCGAGAGGAGTTTGC and GCTGAGA AGATTGGCAGGAC; and *elt-2* forward and reverse—TGCCG ACTTGTATCCCGTTTC and ACTTGGATGTTATCGGCAGGTC. RNA isolation from embryos and qRT-PCR was independently done three times for each stain.

DID-2 and MRP-4 necessity assays

RNAi conditions that reduced DID-2::GFP/MRP-4::GFP levels in *cup-5(zu223)* to wild-type levels were determined by making dilutions of control/pPD129.36 RNAi with varying amounts of *did-2* RNAi or *mrp-4* RNAi feeding bacteria. To measure the DID-2::GFP/MRP-4::GFP levels corresponding to each dilution, seven to nine embryos were imaged for each strain and dilution. The average level of each DID-2::GFP/MRP-4::GFP compartment was determined. At least 25 discrete intracellular structures from each strain and RNAi were used in the measurements. The dilution where the average level of all the DID-2::GFP/MRP-4::GFP compartments measured in *cup-5(zu223)* was not statistically different from the average level of DID-2::GFP/MRP4::GFP compartments in wild type was chosen. Viability tests to measure embryonic viability were concurrently done with the imaging such that RNAi's done for the imaging were done side-by-side with the RNAi's for viability tests.

Western analysis

Adult wild-type and *cup-5(zu223)* hermaphrodites were allowed to lay eggs for 14 hr at 20° to minimize the accumulation of dead embryos laid by *cup-5(zu223)* homozygous parents. Eggs and worms were collected off the plates in M9 buffer and treated with bleach solution to dissolve bacteria and worms and isolate the viable eggs. The embryos were then washed with ddH_2O and lysed for Western analysis.

Pelt-2::GFP Western: After isolation, embryos were suspended in 1× Western Sample Buffer [50 mM Tris, pH 6.8, 10% glycerol, 4% SDS, 10 mM DTT; 1 tablet of complete inhibitor (Life Sciences, Indianapolis) per 1 ml of buffer]. The suspended embryos were freeze-thawed twice (frozen in liquid nitrogen and thawed at 68°) and then boiled for 8 min. Following determination of sample concentrations using Spectra Max 250 (Molecular Devices, Sunnyvale, CA), bromophenol blue was added, and same amounts of total protein of the wild type and *cup-5(zu223)* samples were used for the Western blot.

Pmrp-4::MRP-4::GFP and Pdid-2::DID-2::GFP Western: After isolation, embryos were suspended in Urea/SDS/NP-40 buffer (4% SDS, 1% NP-40, 5% 2-mercaptoethanol, 6 M Urea, 10 mM DTT, 10% glycerol, 0.002% bromophenol blue, 0.05 M Tris–HCl; 1 tablet of complete inhibitor per 1 ml of buffer). The suspended embryos were frozen in liquid nitrogen, thawed, and sonicated using the Bioruptor Standard sonicator (high power for 15 min, 30 sec ON/30 sec OFF). The samples were then left at 37° for 5 min and spun down at 16,000 × *g* for 10 min. Ten microliters of each sample wasloaded for Western analysis.

Pelt-2::DID-2::GFP Western and Pelt-2::MRP-4::GFP Western: After isolation, embryos were suspended in 1× RIPA Buffer (50 mM Tris–HCI, pH 7.4, 150 mM NaCl, 1% NP-40, 0.5% sodium deoxycholate, 1 mM EDTA, 0.1% SDS, 0.42 mg/ml sodium fluoride, 0.368 mg/ml sodium orthovanadate, 12.1 μg/ml ammonium molybdate, 2.4 mM MG132, 2.5 mg/ml *N*-ethylmaleimide; 1 tablet of complete inhibitor per 1 ml of buffer). The suspended embryos were frozen in liquid nitrogen, thawed on ice, and sonicated using the Bioruptor Standard sonicator (high power for 5 min, 30 sec ON/30 sec OFF). Following determination of sample concentrations using Spectra Max 250, 5× Western Sample Buffer was added to the samples. The samples were then put at 70° for 10 min and spun-down at 16,000 × *g* for 10 min. The same amounts of total protein of the wild-type and *cup-5(zu223)* samples were used for the Western blot.

The intensities of the bands were determined using ImageJ. RME-1 was used as a loading control and to normalize values between wild type and *cup-5(zu223)* samples.

DID-2::GFP membrane fractionation

Adult wild-type and *cup-5(zu223)* hermaphrodites were allowed to lay eggs for 14 hr at 20°. Eggs and worms were treated with bleach, and following washes with M9 buffer, the isolated eggs were resuspended in 0.3 ml of membrane lysis buffer (0.2 M Sorbitol, 50 mM KOAc, 2 mM EDTA, 20 mM HEPES–KOH, 1 mM DTT, pH 6.8; 1 tablet of complete inhibitor per 1 ml of buffer). The embryos were then lysed using the Bioruptor Standard sonicator (1 sec at high power followed by 5 sec at low power). The sample was spun-down at 3400 × *g* for 15 min at 4° to remove intact embryos that had not lysed. and the supernatant was preserved for membrane fractionation.

The supernatant was extracted and spun-down at 200,000 × *g* for 60 min at 4°. The pellet was kept as the membrane fraction and was resuspended in 200 μl of 1× Laemmli Buffer–Urea (8% SDS, 2% NP-40, 10% 2-mercaptoethanol, 6 M Urea, 20 mM DTT, 20% glycerol, 0.004% bromophenol blue, 0.1 M Tris–HCl; 1 tablet of complete inhibitor per 1 ml of buffer) and left at 37° for 40 min with occasional mixing by pipetting. The supernatant from the 200,000 × *g* centrifugation represents the cytosolic fraction and was concentrated using a MWCO 3000 microcon (Millipore, Billerica, MA) at 4°. The final volume of the supernatant sample was adjusted to 200 μl in 1× Laemmli buffer–urea, and the sample was incubated at 37° for 10 min. Equal volumes of supernatant and pellet were used for Western analysis.

MRP-4::GFP ubiquitination assay plus or minus RNAi

A total of 1000 adult wild-type, *unc-75(e950) ego-2(om33) arIs37[Pmyo-3::ssGFP; dpy-20]*, *cup-5(zu223)*, or *cup-5(zu223)*; *unc-75(e950) ego-2(om33) arIs37[Pmyo-3::ssGFP; dpy-20]* hermaphrodites carrying the P*elt-2*::*MRP-4*::*GFP* transgene were allowed to lay eggs for 14 hr at 20°. Eggs and worms were treated with bleach solution, and following washes with M9 buffer, the isolate eggs were resuspended in 0.3 ml of ice-cold 1× RIPA Buffer (50 mM Tris–HCl, pH 7.4, 150 mM NaCl, 1% NP-40, 0.5% sodium deoxycholate, 1 mM EDTA, 0.1% SDS, 0.42 mg/ml sodium fluoride, 0.368 mg/ml sodium orthovanadate, 12.1 μg/ml ammonium molybdate, 2.4 mM MG132, 2.5 mg/ml *N*-ethylmaleimide; 1 tablet of complete inhibitor per 1 ml of buffer). The embryos were lysed using the Bioruptor Standard sonicator (high power for 5 min, 30 sec ON/30 sec OFF). The sample was spun-down to remove intact eggs, and the supernatant was transferred to a new tube. Thirty microliters of the supernatant was added to 30 μl of 2× Western Sample Buffer (100 mM Tris, pH 6.8, 20% glycerol, 8% SDS, 20 mM DTT, 20% bromophenol blue; 1 tablet of complete inhibitor per 1 ml of buffer); this was the total protein sample. The remainder of the sample was used for immunoprecipitation.

Immunoprecipitation was done using 20 μl of Sepharose-conjugated anti-GFP beads (Abcam, Cambridge, MA) in Pierce Centrifuge Columns (Rockford, IL). The Sepharose-conjugated anti-GFP beads in 700 μl of 1× RIPA Buffer were added to the columns and then centrifuged at 2875 × *g* for 1 min. The columns were washed two more times with 1× RIPA Buffer. Following the last spin, the supernatant was added to the column and left to mix overnight at 4°. The beads were washed three times with 700 μl of 1× RIPA Buffer (using 1 min 2875 × *g* centrifugation). Immunoprecipitates were eluted using 100 μl of 2× Western Buffer without DTT preheated to 95°. Following elution, 2 μl of 1 M DTT was added to samples that were incubated at 70° for 30 min.

Antibodies and Western detection

Antibodies used in this study were the following: chicken anti-GFP (Abcam); mouse anti-Ubiquitin P4D1 (Santa Cruz Biotechnology, Dallas, TX); mouse anti-Ubiquitin FK1 (Enzo Life Sciences, Farmingdale, NY); mouse anti-RME-1 (Developmental Studies Hybridoma Bank, Iowa City, IA) (Hadwiger *et al.* 2010); mouse anti-LMP-1 (Developmental Studies Hybridoma Bank) (Hadwiger *et al.* 2010); rabbit anti-TagRFP (Abcam); donkey anti-rabbit-IgG-Cy3 (Jackson ImunoResearch Laboratories, West Grove, PA); donkey anti-Chicken-IgY-FITC (Jackson ImmunoResearch Laboratories); donkey anti-chicken IgG-HRP (Jackson ImmunoResearch Laboratories); and goat anti-mouse IgG-HRP (Jackson ImmunoResearch Laboratories).

Western detection was done using the SuperSignal West Dura kit (ThermoFisher Scientific).

Statistical methods

The Student's *t*-test was used to compare average measurements from two samples using a two-tailed distribution (tails = 2) and a two-sample unequal variance (type = 2). Unless otherwise specified, all error bars represent the standard deviation.

Data availability

All data and reagents are available upon request.

Results

Identification of an ESCRT-associated protein suppressor of cup-5(null) lethality

To decipher pathways that lead from loss of CUP-5 to developing intestinal cell death, we began a genome-wide RNA interference (RNAi) feeding screen for suppressors of *cup-5(null)* embryonic lethality (Kamath and Ahringer 2003). We identified *did-2/phi-24/F23C8.6* as a strong suppressor of *cup-5(null)*. While 0% of eggs laid by *cup-5(null)* worms hatched after control RNAi, 79 ± 6% of eggs laid by *cup-5(null)* worms hatched after *did-2* RNAi; viable worms grew to adulthood within 2–3 days of hatching, similar to wild-type worms (RNAi 1 in Figure 1, A and B). This strong suppression of *cup-5(null)* lethality by *did-2* RNAi is similar to the suppression of *cup-5(null)* lethality by the *mrp-4* null allele or *mrp-4* RNAi (Figure 1B) (Schaheen *et al.* 2006b). DID-2 is the *C. elegans* homolog of *S. cerevisiae* Did2p

(37.6% identical) and human CHMP1b (53.2% identical) (Supporting Information, Figure S1A).

We could not use the *did-2(ok3325)* null allele to test for suppression of *cup-5(null)* lethality because homozygous *did-2(ok3325)* is embryonically lethal (Moerman and Barstead 2008). Although the genomic *did-2* RNAi feeding clone included an insert that does not have predicted secondary targets, we designed two other RNAi feeding constructs to confirm that the suppression was due to reduction of *did-2* levels. These two RNAi clones also suppressed *cup-5(null)* lethality, albeit with different efficiencies as has been seen in many other genes (Figure 1, A and B). We used the *did-2* RNAi 1 clone for all of the future experiments.

Reducing levels of did-2 rescues the lysosomal degradation defects of cup-5(null)

cup-5(null) mutants have dysfunctional lysosomes that lead to embryonic lethality and tissue degeneration (Schaheen *et al*. 2006a; Campbell and Fares 2010). To determine whether DID-2 exerts its effects upstream or downstream of the lysosomal defects found in *cup-5(null)* mutants, we looked at lysosomal degradation of the yolk protein VIT-2. VIT-2::GFP is endocytosed by oocytes and subsequently degraded primarily by intestinal cells in developing embryos (Grant and Hirsh 1999).

As we had previously shown, VIT-2::GFP accumulates in larger vacuoles in *cup-5(null)* mutants compared to wild type (Figure 1, C–E) (Schaheen *et al.* 2006a). While RNAi of *did-2* had no significant effect on lysosome size and degradation of VIT-2::GFP in wild-type embryos, RNAi of *did-2* in *cup-5(null)* mutants rescued both the expanded lysosome sizes and the defective degradation of VIT-2::GFP (Figure 1, C–E). This suppression of *cup-5(null)* lysosomal defects after reducing levels of DID-2 indicates that DID-2 protein function is necessary for the development of lysosomal defects in *cup-5(null)* embryonic intestinal cells.

DID-2 protein levels are increased in cup-5(null) mutants

We determined whether alterations to DID-2 levels accounted for the requirement of DID-2 for the lysosomal defects in the absence of CUP-5. We first made transgenic worms that express a functional DID-2::GFP fusion protein under the control of its own *did-2* promoter (Figure S1B). DID-2::GFP localizes to the cytoplasm and to endosomal membranes. Analysis of confocal images of developing intestinal cells in embryos showed that total (membrane bound and cytoplasmic) DID-2::GFP levels were increased in *cup-5(null)* embryos relative to wild-type embryos (Figure 2, A and B). We got similar results using Western analysis on total proteins from mixed-stage embryos (Figure 2C). In these Western blots of total embryonic proteins, DID-2::GFP often appeared as a doublet with a lower band at its expected size of ~49 kDa and an upper band that is 7–10 kDa larger; the levels of both the lower and the upper bands are proportionally increased in the absence of CUP-5 (Figure 2C). RME-1 was used to normalize loading since RME-1 protein levels are the same in wild-type and *cup-5(null)* embryos (Figure S2, A–C).

We then asked whether there was more DID-2::GFP being recruited and bound to endosomal membranes in *cup-5(null)*. Quantitation of the confocal images showed that, individually, both cytoplasmic and membrane-bound DID-2::GFP levels are increased in *cup-5(null)* (Figure 2, A, D, and E). However, there was not a significant difference in the ratio of cytoplasmic DID-2::GFP to membrane-bound DID-2::GFP in wild type (0.62 +/− 0.14) compared to *cup-5(null)* (0.62 ± 0.13) (Figure 2, A and F). This result was confirmed by membrane fractionation where the ratio of DID-2::GFP found in the supernatant (cytoplasmic) to DID-2::GFP in the pellet (membrane bound) was similar in wild-type and *cup-5(null)* embryos (Figure 2G). In addition, the larger sized DID-2::GFP band appeared to be the predominant membrane-bound form of DID-2::GFP in both wild type and *cup-5(null)* embryos (Figure 2G). *C. elegans* LMP-1 is homologous to human Lysosomal-Associated Membrane Protein 1 (LAMP1) and was used to test for proper partitioning of membrane and cytosolic fractions (Figure 2G) (Kostich *et al.* 2000).

To determine whether increased DID-2::GFP levels in the absence of CUP-5 is due to changes in DID-2 protein stability, we expressed DID-2::GFP under the control of the intestine-specific *elt-2* promoter (Fukushige *et al.* 1998); *elt-2* promoter activity is unaffected by the loss of CUP-5 (Figure S2, D–F). If the increase in DID-2::GFP (expressed from the *did-2* promoter) levels in the absence of CUP-5 is due to a defect in DID-2::GFP degradation, we would expect to see the same increase in DID-2::GFP (expressed from the *elt-2* promoter) levels. However, we saw that expression of DID-2::GFP from the *elt-2* promoter resulted in similar expression levels between wild-type and *cup-5(null)* embryos using confocal microscopy and Western analysis (Figure 2, A, H, and I). This indicates that increased DID-2 levels in the absence of CUP-5 are not due to altered degradation of DID-2 protein.

This increase in DID-2 levels is consistent with previous *in vitro* studies that showed that MLIV fibroblasts have altered gene expression, including differential regulation of genes functioning in endosome/lysosome trafficking and lysosome biogenesis (Bozzato *et al.* 2008). The transcription factor EB was found as a key regulator of this differential expression; under conditions of lysosomal dysfunction, transcription factor EB translocates to the nucleus and changes the gene expression profile of lysosomal genes, including *MCOLN1* (Sardiello *et al.* 2009). We used HLH-30, the *C. elegans* ortholog of TFEB, to determine whether the increase in DID-2 protein levels was due to TFEB-mediated transcriptional activation (Lapierre *et al.* 2013). RNAi of *hlh-30* did not affect the increase of DID-2 levels in *cup-5(null)* embryos, indicating that the increase in DID-2 protein levels is not due to a TFEB-mediated defect in transcription, but is rather due to defects in messenger RNA (mRNA) processing, degradation, or translation (Figure S3, A and B).

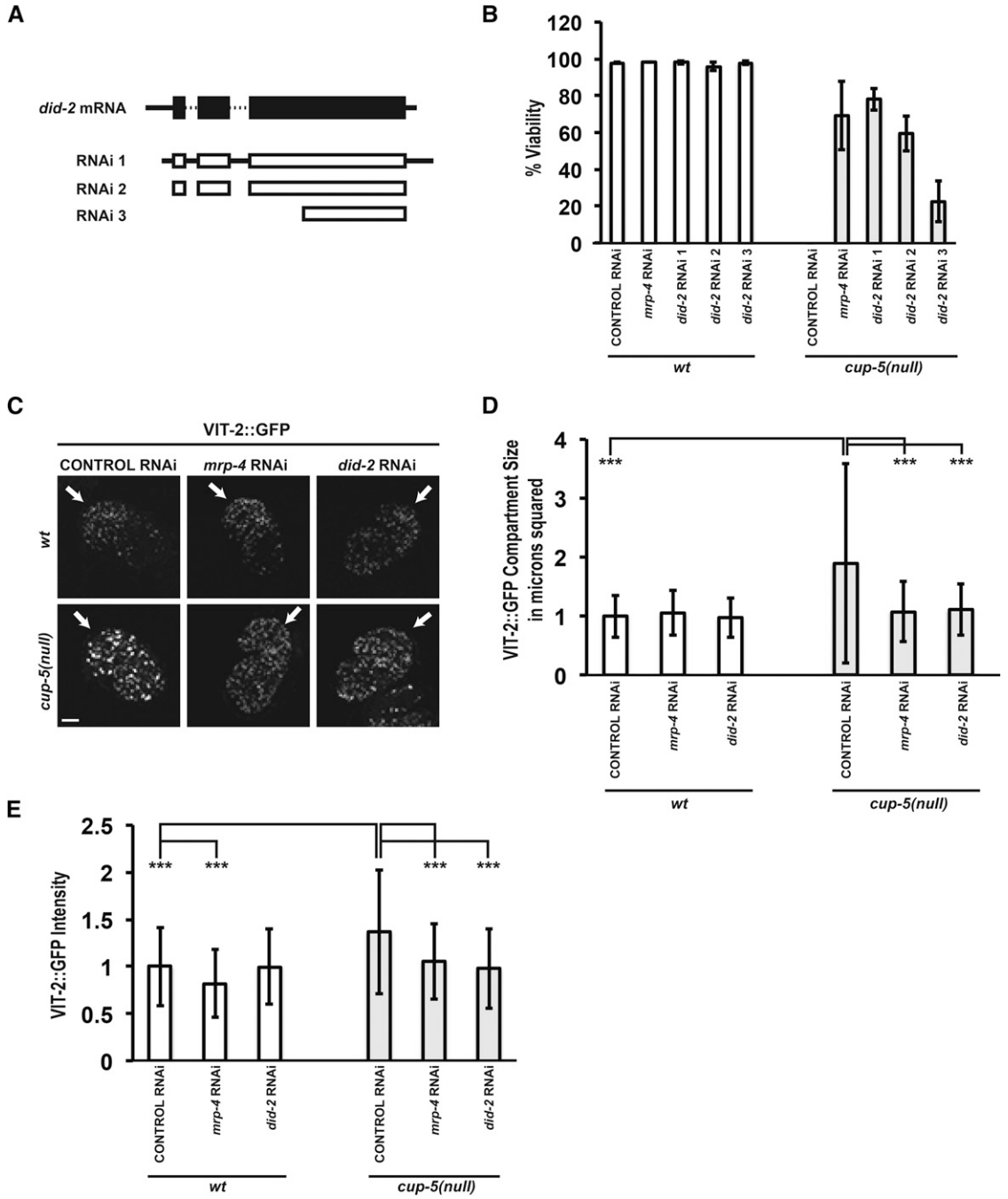

Figure 1 Suppression of *cup-5(null)* defects by RNAi of *did-2*. (A) Structure of *did-2* mRNA (solid black boxes indicate translated regions, solid lines are 5′ and 3′ untranslated regions, and dashed lines are introns) and targeted areas by *did-2* RNAi constructs (RNAi 1–3). (B) Percentage of viable worms laid by wild-type or *cup-5(null)* hermaphrodites after the indicated RNAi's. (C) Confocal images of comma to 1.5-fold stage embryos laid by wild-type or *cup-5(null)* hermaphrodites carrying the VIT-2::GFP transgene after the indicated RNAi's. All images were taken at the same exposure and magnification. Arrows indicate intestinal cells. (D) Quantitation of surface area of VIT-2::GFP compartments in intestinal cells shown in C. (E) Quantitation of the intensity of the VIT-2::GFP compartments in intestinal cells shown in C. Three asterisks indicate $P < 0.0005$. Measurements were normalized to 1 in D and E using the wild-type control RNAi values. Bars in whole-embryo images: 10 μm.

Increased DID-2 levels in cup-5(null) are not sufficient or necessary for cup-5(null) embryonic lethality

To examine the relevance of increased DID-2 levels to *cup-5(null)* lethality, we asked whether this phenotype was sufficient and/or necessary. The DID-2::GFP expressed from the *elt-2* promoter in wild-type embryos is significantly higher than the DID-2::GFP expressed from the *did-2* promoter in *cup-5(null)* embryos (Figure 2, A and B). However, unlike the 100% embryonic lethality of *cup-5(null)* mutants, embryos laid by P*elt-2*::*DID-2*::*GFP* wild-type worms are fully viable.

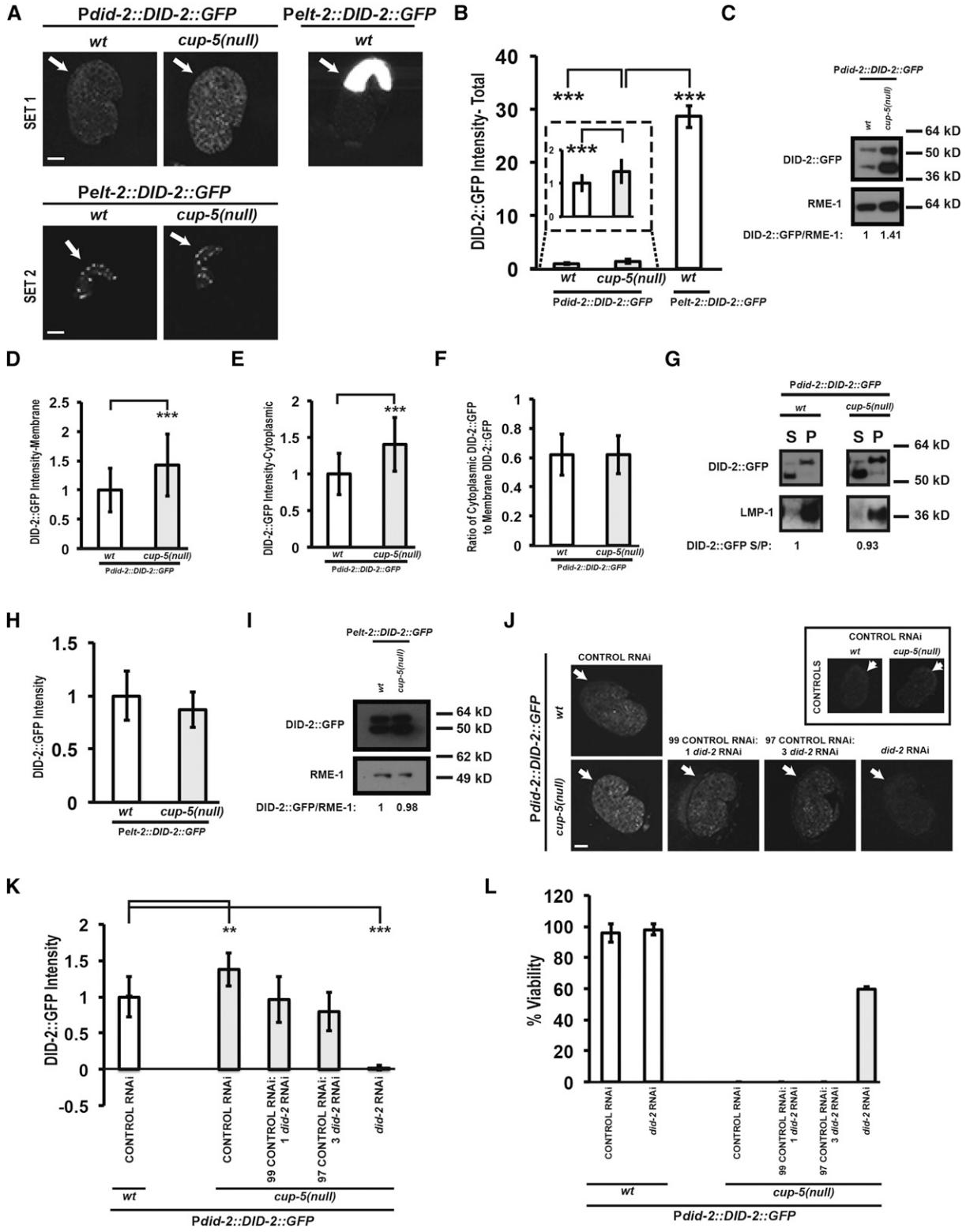

Figure 2 Characterization of DID-2 protein defects in *cup-5(null)*. (A) Confocal images of 1.5-fold stage embryos laid by wild-type (*wt*) and *cup-5(null)* (*zu223* allele) hermaphrodites carrying the DID-2::GFP transgene expressed from the *did-2* promoter or the *elt-2* promoter. All images in set 1 were taken using the same exposure and magnification. All images in set 2 were taken using the same exposure and magnification. Under both of these microscopy conditions, embryos lacking this transgene showed no background fluorescence. Arrows indicate intestinal cells. (B) Quantitation of total DID-2::GFP levels in intestinal cells of wild-type embryos and *cup-5(null)* embryos expressing the indicated fusion protein shown in A, set 1. DID-2::GFP levels expressed from the *elt-2* promoter in wild-type embryos from set 1 is likely higher due to the saturation of the images. (C) Western blot showing DID-2::GFP and RME-1 levels in embryos laid by P*did-2*::*DID-2*::*GFP* wild-type or *cup-5(null)* hermaphrodites. RME-1 was used for normalization. The

This suggests that increased DID-2::GFP levels are not sufficient to cause the embryonic lethality found in *cup-5(null)*. However, the increase in DID-2 levels might still be necessary for *cup-5(null)* lethality.

We identified the RNAi condition that reduced DID-2 levels in *cup-5(null)* mutants to those seen in wild-type embryos; this still resulted in 0% viability in *cup-5(null)* embryos (Figure 2, J–L). Therefore, while increased DID-2 levels is a phenotype seen in the absence of CUP-5, this increase is neither sufficient nor necessary for lethality; the mere presence of DID-2 protein in cells causes cell death in the absence of CUP-5.

Increased MRP-4 levels in cup-5(null) are not due to a defect in MRP-4 degradation rate

DID-2 is a member of the ESCRT complex that targets integral membrane proteins for lysosomal degradation; one of these candidate proteins is the ABC Transporter MRP-4. We had previously shown that reducing levels of MRP-4 in *cup-5(null)* rescues the lysosomal defects in developing intestinal cells and embryonic lethality (Figure 1, C–F) (Schaheen *et al.* 2006b). We had also shown, using a partially functional MRP-4::GFP construct, that MRP-4 levels are elevated in *cup-5(null)* embryos, which we confirmed with a similar partially functional construct using confocal microscopy and Western analysis (Figure 3, A–C) (Schaheen *et al.* 2006b).

We had expected that the increased MRP-4 levels in *cup-5(null)* were caused by a defect in the rate of MRP-4 degradation because of the identification of DID-2 and its ESCRT functions. However, when we assayed for changes in the stability of MRP-4 protein by expressing MRP-4::GFP under the control of the intestine-specific *elt-2* promoter that is unaffected by the loss of CUP-5, we saw that the levels of MRP-4::GFP in wild-type and *cup-5(null)* embryos did not differ using confocal microscopy and Western analysis (Figure 3, D–F). This indicates that the increased levels of MRP-4 protein in *cup-5(null)* are not due to a defect in degradation. In addition, although reducing the levels of the *C. elegans* TFEB ortholog HLH-30 did not suppress the increase in DID-2 protein levels in *cup-5(null)* embryos, we found that *hlh-30* RNAi suppressed the increase in MRP-4 protein levels in *cup-5(null)* embryos (Figure S3, C and D). This suggests that this increase in MRP-4 levels in the absence of CUP-5 is due to HLH-30-mediated transcription. We next asked whether the MRP-4 increased levels were sufficient or necessary for embryonic lethality in *cup-5(null)* worms.

MRP-4 protein increased levels in cup-5(null) are not sufficient or necessary for embryonic lethality

While wild-type P*elt-2*::*MRP-4*::*GFP* embryos have almost seven times increased MRP-4::GFP relative to *cup-5(null)*; P*mrp-4*::*MRP-4*::*GFP* embryos, we could not use these P*elt-2*::*MRP-4*::*GFP* strains to assay sufficiency of MRP-4 overexpression to cause embryonic lethality because MRP-4::GFP is partially functional. Therefore, we made another transgenic strain carrying a P*elt-2*::*MRP-4* transgene that expresses a functional MRP-4 protein because it reverses the suppression of *cup-5(null)* embryonic lethality by the null allele *mrp-4(cd8)* (Figure 3G) (Schaheen *et al.* 2006b). In three independent experiments, quantitative reverse transcription PCR (qRT-PCR) showed that *mrp-4* mRNA levels in the P*elt-2*::*MRP-4* strain are 3, 10, and 21 times higher than nontransgenic strains (Figure 3H). Note that we do not see increased *mrp-4* RNA levels in *cup-5(null)* compared to wild type since a 1.3- to 1.7-fold increase seen in MRP-4::GFP protein levels between these two strains is below the sensitivity of qRT-PCR (Figure 3, A–C and H). Embryos laid from P*elt-2*::*MRP-4* hermaphrodites are 100% viable (Figure 3G). This indicates that increased levels of MRP-4 are not sufficient to cause *cup-5(null)* lethality.

We then assessed the pertinence of increased MRP-4 protein levels for *cup-5(null)* embryonic lethality using the approach that we used to study DID-2 necessity. We identified the RNAi conditions that would reduce MRP-4 levels in *cup-5(null)* mutants to the levels found in wild-type embryos (Figure 3, I and J). Reduction of MRP-4 levels down to the levels seen in wild-type worms still resulted in 0% viability in *cup-5(null)* embryos (Figure 3, I–K). Indeed, even reducing

total of both DID-2::GFP bands was used for the quantitation. (D) Quantitation of membrane-bound DID-2::GFP levels in intestinal cells of P*did-2*::*DID-2*::*GFP* wild-type and *cup-5(null)* embryos hermaphrodites shown in A. (E) Quantitation of cytoplasmic DID-2::GFP in intestinal cells of P*did-2*::*DID-2*::*GFP* wild-type and *cup-5(null)* embryos laid by hermaphrodites shown in A. (F) Quantitation of the ratio of cytoplasmic DID-2::GFP to membrane-bound DID-2::GFP in intestinal cells of P*did-2*::*DID-2*::*GFP* wild-type and *cup-5(null)* embryos laid by hermaphrodites shown in A. (G) Membrane-bound DID-2::GFP (pellet) was separated from cytoplasmic DID-2::GFP (supernatant) in embryos laid by P*did-2*::*DID-2*::*GFP*, wild-type, or *cup-5(null)* hermaphrodites. DID-2::GFP and LMP-1 protein were then detected by Western analysis. DID-2::GFP S/P represents the ratio of cytoplasmic DID-2::GFP to membrane-bound DID-2::GFP; the total of both DID-2::GFP bands was used for the quantitation. LMP-1 protein was used as a control of fractionation. (H) Quantitation of DID-2::GFP levels in intestinal cells of wild-type and *cup-5(null)* embryos laid by P*elt-2*::*DID-2*::*GFP* hermaphrodites shown in A, set 2. (I) Western blot showing DID-2::GFP and RME-1 levels in embryos laid by P*elt-2*::*DID-2*::*GFP* wild-type or *cup-5(null)* hermaphrodites. Equal amounts of total protein levels were loaded. RME-1 was used for normalization. The total of both DID-2::GFP bands were used for the quantitation. (J) Confocal images of comma to 1.5-fold stage embryos laid by P*did-2*::*DID-2*::*GFP* wild-type or *cup-5(null)* hermaphrodites after the indicated RNAi's. The ratios of control RNAi to *did-2* RNAi represent two dilutions of the *did-2* RNAi bacterial seeding clone with the control RNAi bacterial seeding clone. All images were taken using the same exposure and magnification. Arrows indicate intestinal cells. The boxed images are autofluorescence controls of embryos that do not carry the P*did-2*::*DID-2*::*GFP* transgene. (K) Quantitation of DID-2::GFP intensity in intestinal cells after the indicated RNAi's of embryos shown in J. (L) Percentage of embryos laid by P*did-2*::*DID-2*::*GFP* wild-type or *cup-5(null)* hermaphrodites that hatched after the indicated RNAi's shown in J. Two asterisks indicate $P < 0.005$; three asterisks indicate $P < 0.0005$. Measurements were normalized to 1 in B, D, E, H, and K using the wild type or wild-type control RNAi values. Bars, 10 μm in all images.

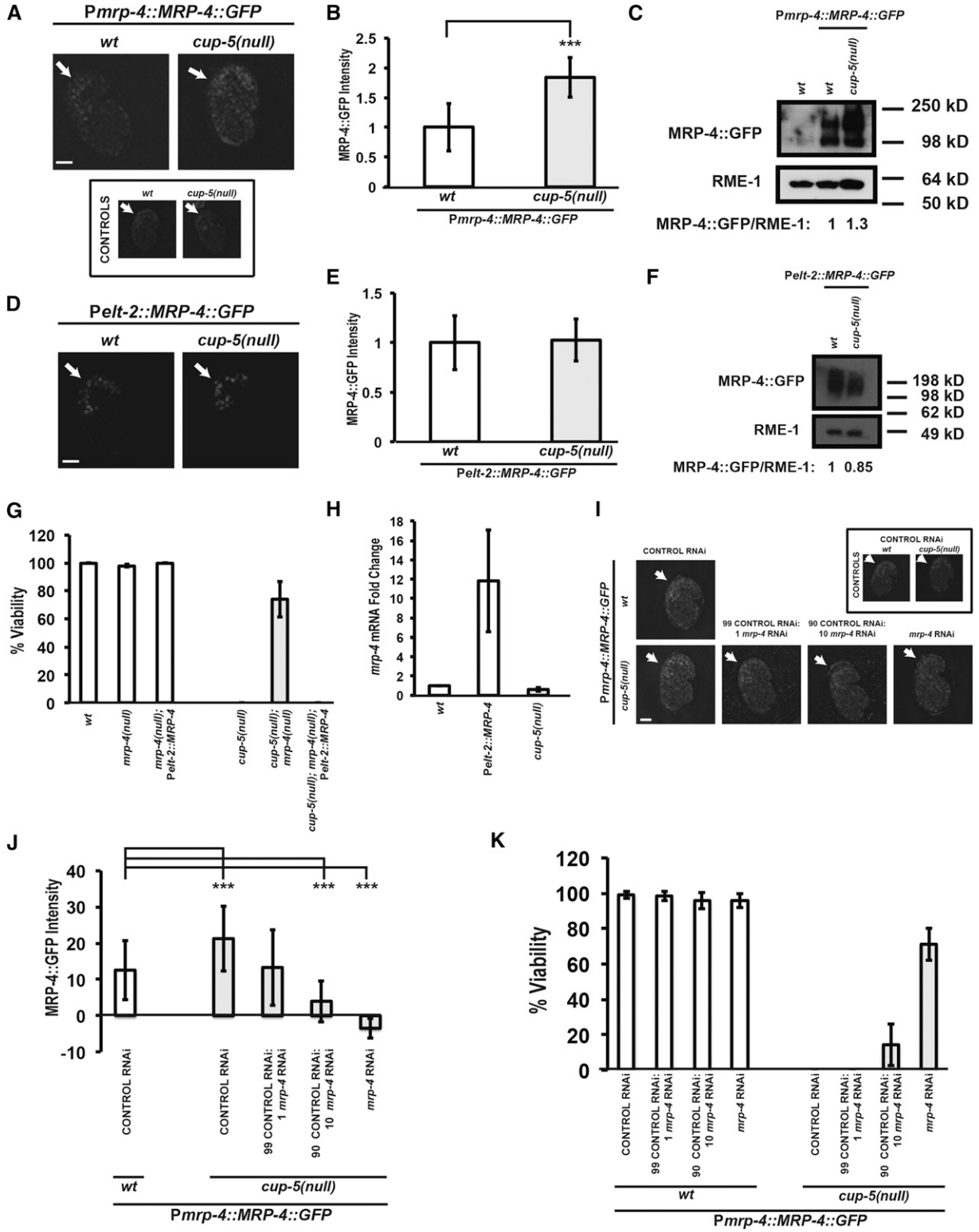

Figure 3 Characterization of MRP-4 protein defects in *cup-5(null)*. (A) Confocal images of 1.5-fold stage embryos laid by wild type (*wt*) and *cup-5(null)* (*zu223* allele) hermaphrodites carrying the MRP-4::GFP transgene expressed from the native *mrp-4* promoter. All images were taken using the same exposure and magnification. Arrows indicate intestinal cells. (B) Quantitation of MRP-4::GFP levels in intestinal cells shown in A. Background immunofluorescence values from wild type and *cup-5(null)* not carrying the MRP-4::GFP transgene were subtracted. (C) Western blot showing MRP-4::GFP and RME-1 levels in embryos laid by P*mrp-4*::*MRP-4*::*GFP* wild-type or *cup-5(null)* hermaphrodites. RME-1 was used for normalization. (D) Confocal images of 1.5-fold stage embryos laid by wild-type and *cup-5(null)* hermaphrodites carrying the MRP-4::GFP transgene expressed from the *elt-2* promoter. All images were taken using the same exposure and magnification. Arrows indicate intestinal cells. Under these microscopy conditions,

cup-5(null) MRP-4 levels down to half the amount in wild type gives only a very slight rescue of lethality (Figure 3, I–K). Thus, the increased levels of MRP-4 are not necessary for the lethality, meaning that the presence of wild-type (or lower) levels of MRP-4 protein in *cup-5(null)* embryos is sufficient to cause embryonic lethality. Since the levels of MRP-4 protein in *cup-5(null)* are not necessary for lethality, we tested whether *did-2* RNAi suppression is mediated by altering the localization of MRP-4 protein.

did-2 RNAi suppression of cup-5(null) defects is not caused by altered localization of MRP-4 protein

Immunofluorescence of embryos expressing a functional DID-2::RFP and MRP-4::GFP showed that, while the staining patterns of these two proteins were fairly different, there was still extensive overlap (Figure 4, A and B). MRP-4::GFP stains whole membranes of compartments, while DID-2::RFP appears to stain punctate microdomains on the same membranes or adjacent compartments (Figure 4, A and B). These results indicate that MRP-4 and DID-2 localize close to each other on endosomes/lysosomes, consistent with MRP-4 protein being a substrate for DID-2/ESCRT functions (see below).

Reducing levels of *did-2* might rescue *cup-5(null)* lethality by shuttling MRP-4 protein away from late endosomes/lysosomes where MRP-4's increased transport activity is damaging to these compartments. We therefore first assayed MRP-4 protein localization in the endo-lysosomal pathway in wild-type and *cup-5(null)* embryos. MRP-4::GFP colocalizes with LMP-1::RFP, a lysosomal membrane marker in wild type and *cup-5(null)*, with no difference in percentage of colocalization of the two proteins between wild type and *cup-5(null)* (Figure 4, C and D) (Campbell and Fares 2010). Thus, MRP-4 protein trafficks through the endo-lysosomal system. We then assayed MRP-4 protein trafficking in the recycling pathway by looking at its localization with *RBB-11.1*::RFP, a marker for recycling endosomes. We saw no MRP-4 protein colocalized with the *RBB-11.1* recycling endosomes in wild-type and *cup-5(null)* embryos, indicating that MRP-4 does not typically get trafficked through the recycling pathway (Figure 4, E and F).

Given MRP-4 protein's presence in the endo-lysosomal pathway and absence in the recycling pathway, we asked whether RNAi of *did-2* rescued *cup-5(null)* lethality by trafficking MRP-4 to the recycling pathway or at the least away from lysosomes where its activity is damaging. RNAi of *did-2* still resulted in no colocalization between MRP-4::GFP and *RBB-11.1*::RFP in wild type and *cup-5(null)*, indicating that *did-2* RNAi rescue was not due to moving MRP-4 protein to the recycling pathway (Figure 4, G and H). Additionally, RNAi of *did-2* did not result in less MRP-4 protein trafficking through the endo-lysosomal system since we did not see lower colocalization between MRP-4::GFP and LMP-1::RFP in *cup-5(null)* after RNAi of *did-2*; in fact, there was a slight increase in colocalization between the proteins (Figure 4, G and H). This indicates that *did-2* RNAi does not rescue *cup-5(null)* defects by altering the endo-lysosomal localization of MRP-4 protein. We then assayed whether *cup-5(null)* lethality and *did-2* RNAi rescue was due to alterations in MRP-4 protein.

MRP-4 protein is hypo-ubiquitinated in cup-5(null)

DID-2 is a member of the ESCRT-associated complex that is required for the de-ubiquitination of integral membrane proteins prior to the completion of the internalization of these integral membrane proteins in intraluminal vesicles. We therefore assayed whether the loss of CUP-5 resulted in perturbations to MRP-4 ubiquitination. We immunoprecipitated MRP-4::GFP out of total protein isolates from wild-type and *cup-5(null)* embryos and determined the fraction of both mono- and poly-ubiquitinated MRP-4::GFP in Western blots using the P4D1 antibody. We found that MRP-4 protein is hypo-ubiquitinated in *cup-5(null)* embryos; at steady state, MRP-4 in *cup-5(null)* shows a significant decrease in ubiquitination to ~35–57% of the levels seen in wild-type embryos (Figure 5, A and B).

Mono-ubiquitination is the signal for cargo entry into the ESCRT pathway (Katzmann *et al.* 2001; Reggiori and Pelham 2001). We used the FK1 antibody, which detects only poly-ubiquitin to assess whether MRP-4 protein is mono- or poly-ubiquitinated. Similar to the P4D1 antibody, the FK1 antibody also detects many proteins that are ubiquitinated in total embryonic lysates (Figure 5B). However, unlike P4D1, FK1 did not detect poly-ubiquitinated immunoprecipitated MRP-4::GFP in wild-type or *cup-5(null)* embryos (Figure 5B). This suggests that MRP-4 protein is mono-ubiquitinated at a lower level in *cup-5(null)* embryos. Therefore, we assayed whether the *cup-5(null)* hypo-ubiquitination was dependent on the presence of DID-2 protein.

embryos lacking this transgene showed no background fluorescence. (E) Quantitation of MRP-4::GFP levels in intestinal cells shown in D. (F) Western blot showing MRP-4::GFP and RME-1 levels in embryos laid by P*elt-2*::*MRP-4*::*GFP* wild-type or *cup-5(null)* hermaphrodites. Equal amounts of total protein levels were loaded. RME-1 was used for normalization. (G) Percentage of viable worms laid by hermaphrodites with the indicated genotypes. (H) Fold-change of *mrp-4* mRNA levels in P*elt-2*::*MRP-4* and *cup-5(null)* relative to wild-type embryos as determined by qRT-PCR. Error bars represent the standard error of the mean. (I) Confocal images of 1.5-fold stage embryos laid by P*mrp-4*::*MRP-4*::*GFP* wild-type or *cup-5(null)* hermaphrodites after the indicated RNAi's. The ratios of control RNAi to *mrp-4* RNAi represent two dilutions of the *mrp-4* RNAi bacterial seeding clone with the control RNAi bacterial seeding clone. All images were taken using the same exposure and magnification. Arrows indicate intestinal cells. (J) Quantitation of MRP-4::GFP puncta intensity in intestinal cells shown in G. (K) Percentage of embryos laid by P*mrp-4*::*MRP-4*::*GFP* wild-type or *cup-5(null)* hermaphrodites that hatched after the indicated RNAi's shown in G. Three asterisks indicate $P < 0.0005$. Measurements were normalized to 1 in B, E, and H using the wild type or wild-type control RNAi values. Bars, 10 μm in all images.

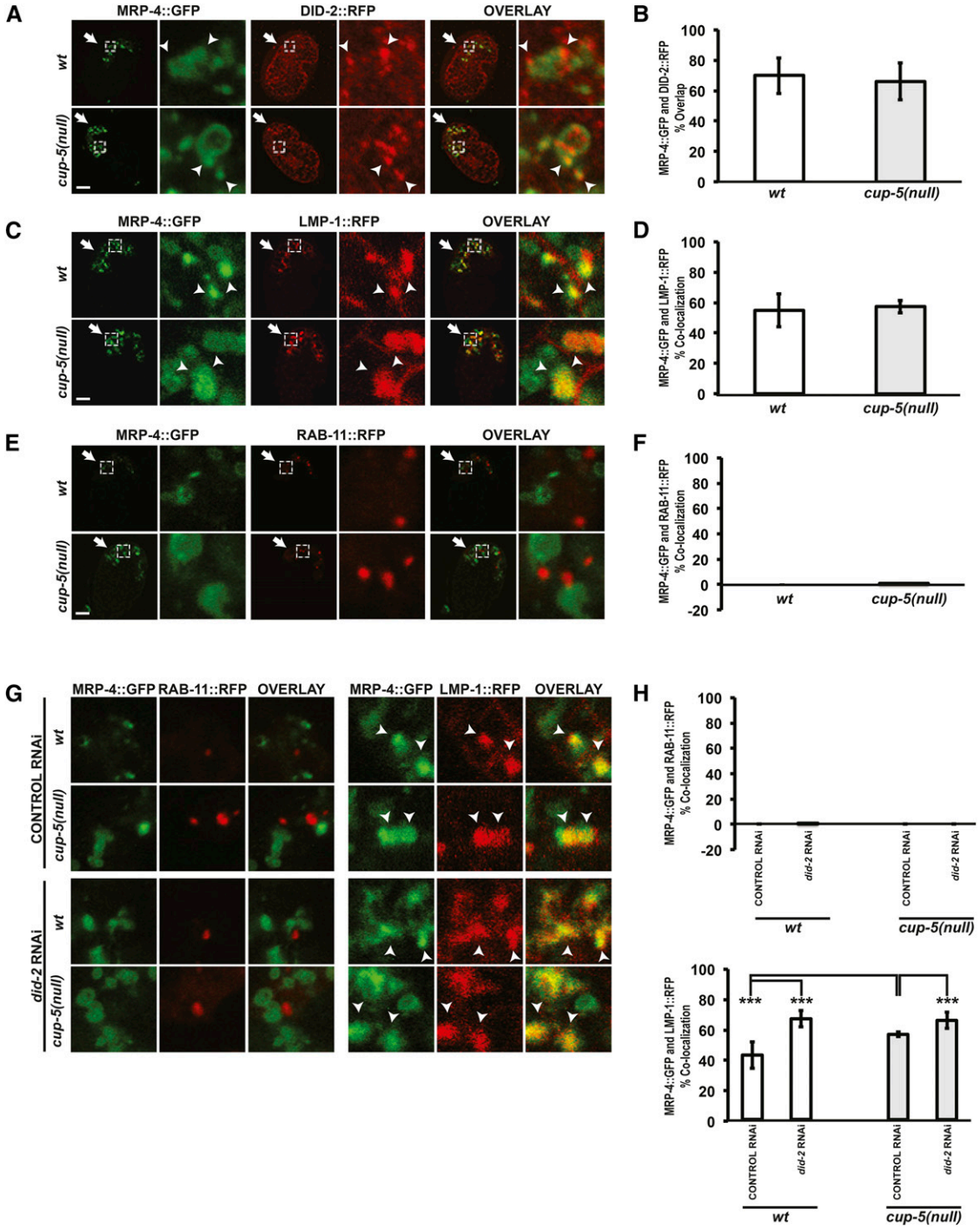

Figure 4 MRP-4 protein localization in wild type and *cup-5(null)*. (A) Confocal images of comma to 1.5-fold stage embryos laid by wild type (*wt*) or *cup-5(null)* (*zu223* allele) hermaphrodites that were immunostained to detect DID-2::RFP and MRP-4::GFP. Arrows indicate intestinal cells. Arrowheads indicate overlap between DID-2::RFP and MRP-4::GFP. Images to the right of the embryos are magnified images of the regions indicated by the dashed white boxes. (B) Quantitation of DID-2::RFP and MRP-4::GFP percent overlap in intestinal cells shown in A. (C) Confocal images of 1.5-fold stage embryos laid by wild-type or *cup-5(null)* hermaphrodites expressing MRP-4::GFP and LMP-1::RFP. Arrows indicate intestinal cells. Arrowheads indicate colocalization between MRP-4::GFP and LMP-1::RFP. Images to the right of the embryos are magnified images of the regions indicated by the dashed white boxes. (D) Quantitation of MRP-4::GFP and LMP-1::RFP percentage of colocalization in intestinal cells shown in C. (E) Confocal images of 1.5-fold embryos laid by wild-type or *cup-5(null)* hermaphrodites expressing MRP-4::GFP and *RBB-11.1*::RFP. Arrows indicate intestinal cells. Images to the right of the embryos are magnified images of the regions indicated by the dashed white boxes. (F) Quantitation of MRP-4::GFP and *RBB-11.1*::RFP percentage of colocalization in intestinal cells shown in E. (G) Confocal images of comma to 1.5-fold stage embryos laid by wild-type and *cup-5(null)* hermaphrodites expressing MRP-4::GFP and LMP-1::RFP or *RBB-11.1*::RFP after the indicated RNAi's. Only the magnified images are shown. Arrowheads indicate colocalization. (H) Quantitation of MRP-4::GFP and LMP-1::RFP percentage of colocalization and MRP-4::GFP and *RBB-11.1*::RFP percentage of colocalization in intestinal cells shown in G. Three asterisks indicate $P < 0.0005$. Bars in whole-embryo images: 10 μm.

Hypo-ubiquitination in cup-5(null) is rescued by reducing levels of did-2

We assayed MRP-4 ubiquitination in wild-type and *cup-5(null)* embryos after RNAi of *did-2*. We saw a fivefold increase in MRP-4 ubiquitination at steady state after *did-2* RNAi in wild-type embryos (Figure 5C). This is consistent with DID-2's function: recruitment of the de-ubiquitinating enzyme to endosomal membranes where it can act on MRP-4 (Row *et al.* 2007). Similarly, there was an increase in MRP-4 ubiquitination at steady state in *cup-5(null)* embryos after RNAi of *did-2* compared to *cup-5(null)* embryos after the control RNAi (Figure 5D). This increase indicates that the hypo-ubiquitination of MRP-4 in *cup-5(null)* developing intestinal cells in embryos is dependent on DID-2 protein and suggests the involvement of other ESCRT-associated proteins in this MRP-4 ubiquitination defect.

Reducing levels of other ESCRT-associated proteins also suppress embryonic lethality, lysosomal defect, and MRP-4 hypo-ubiquitination in cup-5(null)

We tested members of the ESCRT complex for RNAi suppression of *cup-5(null)* embryonic lethality. With the exception of *vps-32.1/C56C10.3*, RNAi of ESCRT genes did not cause significant lethality of wild-type embryos (Figure 6A). RNAi of *hgrs-1*, an ESCRT-0 protein, gave 38.8 ± 14.48% rescue of *cup-5(null)* embryonic lethality, although RNAi of the other ESCRT-0 gene, *stam-1*, gave no rescue (Figure 6A). In addition, RNAi of *vps-2* (ESCRT-II) and *vps-4* (ATPase complex) gave weak rescue of *cup-5(null)* lethality (Figure 6A).

We saw the strongest rescue of *cup-5(null)* lethality after RNAi of the ESCRT-associated genes *usp-50*, *ego-2*, and *alx-1* (Figure 6A). USP-50 is the *C. elegans* homolog of *S. cerevisiae* Doa4p and human USP8/UBPY and EGO-2 and its homolog ALX-1 are the *C. elegans* homologs of human HD-PTP and Alix, respectively, and of *S. cerevisiae* Bro1p. While 0% of eggs laid by *cup-5(null)* hermaphrodites hatch, RNAi of *usp-50* gave 76 ± 15.6% viability (Figure 6A). RNAi of *ego-2* alone in *cup-5(null)* gave 26 ± 5.14% viability while RNAi of *alx-1* gave no rescue of lethality (Figure 6A). RNAi of *ego-2*+*alx-1* in *cup-5(null)* gave 16 ± 11.1% viability [which was not significantly different from the viability after RNAi of *ego-2* alone in *cup-5(null)*; $P > 0.05$] (Figure 6A). However, because combination RNAi's are not as effective as single RNAi's, and since EGO-2 and ALX-1 may have redundant ESCRT functions, we tested the *ego-2*+*alx-1* RNAi in the presence of an *ego-2(om33)* hypomorphic allele that reduces EGO-2 activity. Indeed, RNAi of *ego-2*+*alx-1* results in 81.17 ± 11.05% viability in the *cup-5(null)*; *ego-2(om33)* background (Figure 6B).

Because of their strong suppression of *cup-5(null)* lethality, we focused our analysis on these ESCRT-associated proteins. We first assayed the degradation of VIT-2::GFP after reducing levels of these ESCRT-associated proteins in embryos laid by *cup-5(null)* hermaphrodites. Reducing levels of USP-50 suppresses both the *cup-5(null)* degradation defect and expanded lysosome size (Figure 6, C–E). Similarly, reducing levels of EGO-2+ALX-1 also suppresses the degradation defect and the expanded lysosome size in the *cup-5(null)* background (Figure 6, C–E). Similar to what we observed with DID-2 and MRP-4 proteins, these results indicate that the presence of USP-50 and ALX-1+EGO-2 is required for the appearance of the lysosomal defect in the absence of CUP-5.

The rescue of *cup-5(null)* lethality and the lysosomal defect by reducing levels of USP-50 and EGO-2+ALX-1 is not due to altering the endo-lysosomal localization of MRP-4 protein. Reducing levels of USP-50 in the *cup-5(null)* background resulted in an increase, rather than a decrease, in colocalization between MRP-4::GFP and LMP-1::RFP, while RNAi of *alx-1*+*ego-2* resulted in no significant change in colocalization between the two proteins (Figure S4, A and B). This indicates that RNAi of these genes does not rescue *cup-5(null)* defects by trafficking MRP-4 protein away from the endo-lysosomal system where it does its damage.

We then assayed hypo-ubiquitination of MRP-4 protein in *cup-5(null)* to assess whether it was dependent on the presence of USP-50 or EGO-2+ALX-1. RNAi of *usp-50* increases MRP-4 protein ubiquitination 7.7-fold at steady state in wild-type embryos when compared with control RNAi, consistent with its de-ubiquitinating activity (Figure 5C). This increase in MRP-4 ubiquitination is also seen after RNAi of *usp-50* in *cup-5(null)* embryos at steady state with a 3.7-fold increase from control RNAi, establishing that *cup-5(null)* hypo-ubiquitination is dependent on USP-50 protein activity (Figure 5D). While RNAi of *alx-1*+*ego-2* increases MRP-4 ubiquitination at steady state in wild-type embryos compared to control RNAi, we did not see an increase in MRP-4 ubiquitination in *cup-5(null)* embryos when compared to control RNAi (Figure 5, C and D). However, in the presence of the *ego-2(om33)* hypomorphic allele, reducing levels of *alx-1*+*ego-2* increases MRP-4 protein ubiquitination at steady state in wild type (2.4-fold) and *cup-5(null)* (1.5-fold) embryos when compared with control RNAi (Figure 5, E and F).

ESCRT-associated/MRP-4 RNAi rescue of cup-5(null) lysosomal defects shows tissue and developmental specificity

Is this genetic pathway linking ESCRT-associated proteins and MRP-4 with CUP-5 seen in developing intestinal cells in embryos also present in other tissues and at other stages of development? We first assayed GFP that is secreted by muscle cells and that is then endocytosed by coelomocytes; the GFP accumulates in terminal compartments (lysosomes) of the coelomocytes (Treusch *et al.* 2004). We measured GFP-filled compartment sizes because the intensity of endocytosed GFP in *cup-5(null)* coelomocytes was very bright compared to wild type and was saturated at the microscopy settings used to visualize wild-type coelomocytes. As we had previously shown, the GFP-filed compartments are larger in adult *cup-5(null)* compared to adult wild-type coelomocytes, indicating a lysosomal defect in the absence of CUP-5 (Figure S5, A–C) (Fares and Greenwald 2001b). RNAi of *did-2*, *usp-50*, *alx-1*+*ego-2*, or *mrp-4* does not rescue this increased

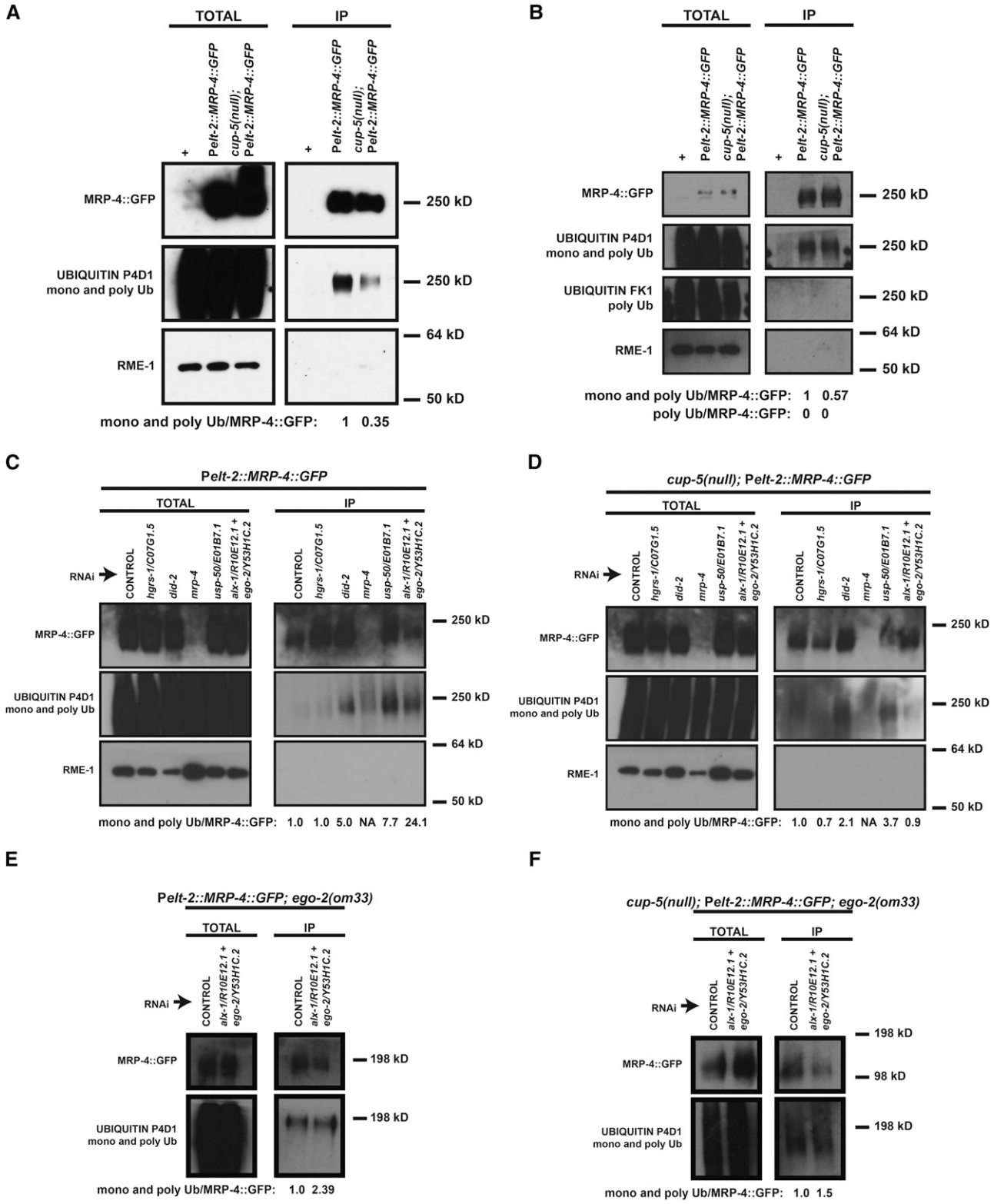

Figure 5 MRP-4 protein ubiquitination in wild type and *cup-5(null)*. (A) Western blots probing for MRP-4::GFP, ubiquitin, and RME-1 protein in embryos laid by P*elt-2*::*MRP-4*::*GFP*, wild-type, or *cup-5(null)* hermaphrodites. (Left) Total protein isolates. (Right) Total protein isolates after immunoprecipitation of MRP-4::GFP. The P4D1 antibody was used to detect ubiquitin; this antibody detects both mono- and poly-ubiquitination. Ub/MRP-4::GFP represents the fraction of MRP-4 that is ubiquitinated. The plus sign (+) indicates control wild-type worms that do not carry the P*elt-2*::*MRP-4*::*GFP* transgene. (B) Western blots probing for MRP-4::GFP, ubiquitin, and RME-1 protein in embryos laid by P*elt-2*::*MRP-4*::*GFP*, wild-type, or *cup-5(null)* hermaphrodites. (Left) Total protein isolates. (Right) Total protein isolates after immunoprecipitation of MRP-4::GFP. In addition to the P4D1 antibody, the FK1 antibody was used to specifically detect poly-ubiquitin. Ub/MRP-4::GFP represents the fraction of MRP-4 that is ubiquitinated. The plus sign (+) indicates control

compartment size in adult *cup-5(null)* coelomocytes (Figure S5, A–C). Indeed, while RNAi of the ESCRT-associated proteins did not significantly alter the GFP-filled compartment sizes of adult wild-type coelomocytes, RNAi of *did-2* and *alx-1*+*ego-2* significantly increased GFP-filled compartment sizes of adult *cup-5(null)* coelomocytes (Figure S5, A–C). Thus, the suppression of *cup-5(null)* lysosomal defects by RNAi of ESCRT-associated proteins or MRP-4 in developing intestinal cells in embryos does not occur in adult coelomocytes.

We then assayed the adult intestine to determine whether RNAi of ESCRT-associated proteins or MRP-4 rescues lysosomal defects in intestinal cells of adult *cup-5(null)* worms. The levels of the lysosomal marker, LMP-1::GFP, are increased in the adult intestine of *cup-5(null)* hermaphrodites compared to wild type, indicating a lysosomal defect in the absence of CUP-5 (Figure 7, A–C). RNAi of *did-2*, *usp-50*, *alx-1*+*ego-2*, and *mrp-4* cause an increase in LMP-1::GFP levels in wild-type adult intestines, consistent with their functioning in this tissue. However, RNAi of these ESCRT-associated proteins or MRP-4 did not rescue the increased LMP-1::GFP levels in *cup-5(null)* adults (Figure 7, A–C). Thus, this genetic pathway that is evident in embryonic intestinal cells is absent in adult intestinal cells.

Taken together, the data suggest that *cup-5(null)* suppression by RNAi of the ESCRT-associated proteins and MRP-4 exhibits tissue and developmental specificity.

Discussion

In this study, we uncover a novel genetic link between CUP-5 and ESCRT-associated proteins. Our model is that the absence of CUP-5 results in increased activity of the deubiquitinating enzyme USP-50, as evidenced by the suppression of *cup-5(null)* defects after reducing the levels of the ESCRT-associated proteins DID-2, USP-50, or ALX-1+EGO-2. Our results also suggest that this ESCRT-associated defect impacts lysosomal functions and embryonic lethality in the absence of CUP-5 at least in part through affecting the activity of the ABC transporter MRP-4 and possibly by altering the levels and/or activities of other proteins.

We found that the loss of CUP-5 resulted in increases in levels of DID-2 and MRP-4 proteins. The increase in DID-2 levels is not due to altered degradation or TFEB-mediated transcriptional activation in the absence of CUP-5. In contrast, our studies suggest that the increase in MRP-4 levels is due to altered transcription that is mediated by HLH-30/TFEB. However, other studies have shown that, under lysosomal stress conditions, Ca^{2+} released from lysosomes by TRPML1 causes the translocation of TFEB to the nucleus where it activates transcription (Medina *et al.* 2015). Therefore, how does HLH-30 translocate to the nucleus to increase transcription of *mrp-4* when CUP-5 is not present to release Ca^{2+} from lysosomes? Our model is that the lysosomal defect in the absence of CUP-5 leads to lysosome rupture or leakiness, thus releasing Ca^{2+} into the cytoplasm. Indeed, the lysosomal protease Cathepsin B has been found to leak into the cytoplasm after severe knockdown of TRPML1 in HeLA cells (Colletti *et al.* 2012).

Although we detect changes in the levels of DID-2 and MRP-4 in the absence of CUP-5, our results show that the increased levels of these proteins do not contribute to *cup-5(null)* lethality. Therefore, while these gene expression changes are phenotypes of *cup-5(null)* tissues, they do not impact lysosomal functions or tissue viability. Which phenotypes, then, are relevant?

We propose that the hypo-ubiquitination of MRP-4 protein in *cup-5(null)* is a major contributor to the lysosomal and viability defects since both defects are rescued by reducing the levels of ESCRT-associated proteins, including the catalytic enzyme USP-50. Surprisingly, given the established functions of ESCRT proteins in shuttling receptors for degradation, this hypo-ubiquitination of MRP-4 in the absence of CUP-5 had no effect on the levels of MRP-4 protein. Our model is that the mono-ubiquitin state of MRP-4 protein modulates its activity, where hypo-ubiquitination of MRP-4 results in increased MRP-4 transporter activity leading to lysosomal defects and ultimately to tissue death. In addition, since overexpression of MRP-4 is not sufficient to cause embryonic lethality, this suggests that the mono-ubiquitination of MRP-4 is used to regulate the total transporter activity of MRP-4 in late endosomes/lysosomes, irrespective of how much MRP-4 protein is present in these compartments. Our results show that CUP-5 directly or indirectly regulates the activity of the ESCRT-associated proteins such that loss of CUP-5 results in their mis-regulation. The question then

wild-type worms that do not carry the P*elt-2*::*MRP-4*::*GFP* transgene. (C) Western blots probing for MRP-4::GFP, ubiquitin, and RME-1 protein in embryos laid by P*elt-2*::*MRP-4*::*GFP* wild-type hermaphrodites after the indicated RNAi's. (Left) Total protein isolates. (Right) Total protein isolates after immunoprecipitation of MRP-4::GFP. The P4D1 antibody was used to detect ubiquitin; this antibody detects both mono- and poly-ubiquitination. Ub/MRP-4::GFP represents the fraction of MRP-4::GFP that is ubiquitinated. (D) Western blots probing for MRP-4::GFP, ubiquitin, and RME-1 protein in embryos laid by *cup-5(null)*; P*elt-2*::*MRP-4*::*GFP* hermaphrodites after the indicated RNAi's. (Left) Total protein isolates. (Right) Total protein isolates after immunoprecipitation of MRP-4::GFP. Ub/MRP-4::GFP represents the fraction of MRP-4::GFP that is ubiquitinated. (E) Western blots probing for MRP-4::GFP and ubiquitin in embryos laid by *ego-2(om33)*; P*elt-2*::*MRP-4*::*GFP* hermaphrodites after the indicated RNAi's. (Left) Total protein isolates. (Right) Total protein isolates after immunoprecipitation of MRP-4::GFP. Ub/MRP-4::GFP represents the fraction of MRP-4::GFP that is ubiquitinated. (F) Western blots probing for MRP-4::GFP and ubiquitin in embryos laid by *cup-5(null)*; *ego-2(om33)*; P*elt-2*::*MRP-4*::*GFP* hermaphrodites after the indicated RNAi's. (Left) Total protein isolates. (Right) Total protein isolates after immunoprecipitation of MRP-4::GFP. Ub/MRP-4::GFP represents the fraction of MRP-4::GFP that is ubiquitinated. Measurements were normalized to 1 in A–F using the wild type, wild-type control RNAi, or *cup-5(null)* control RNAi Ub/MRP-4::GFP values. RME-1 was used to confirm MRP-4::GFP enrichment following immunoprecipitation.

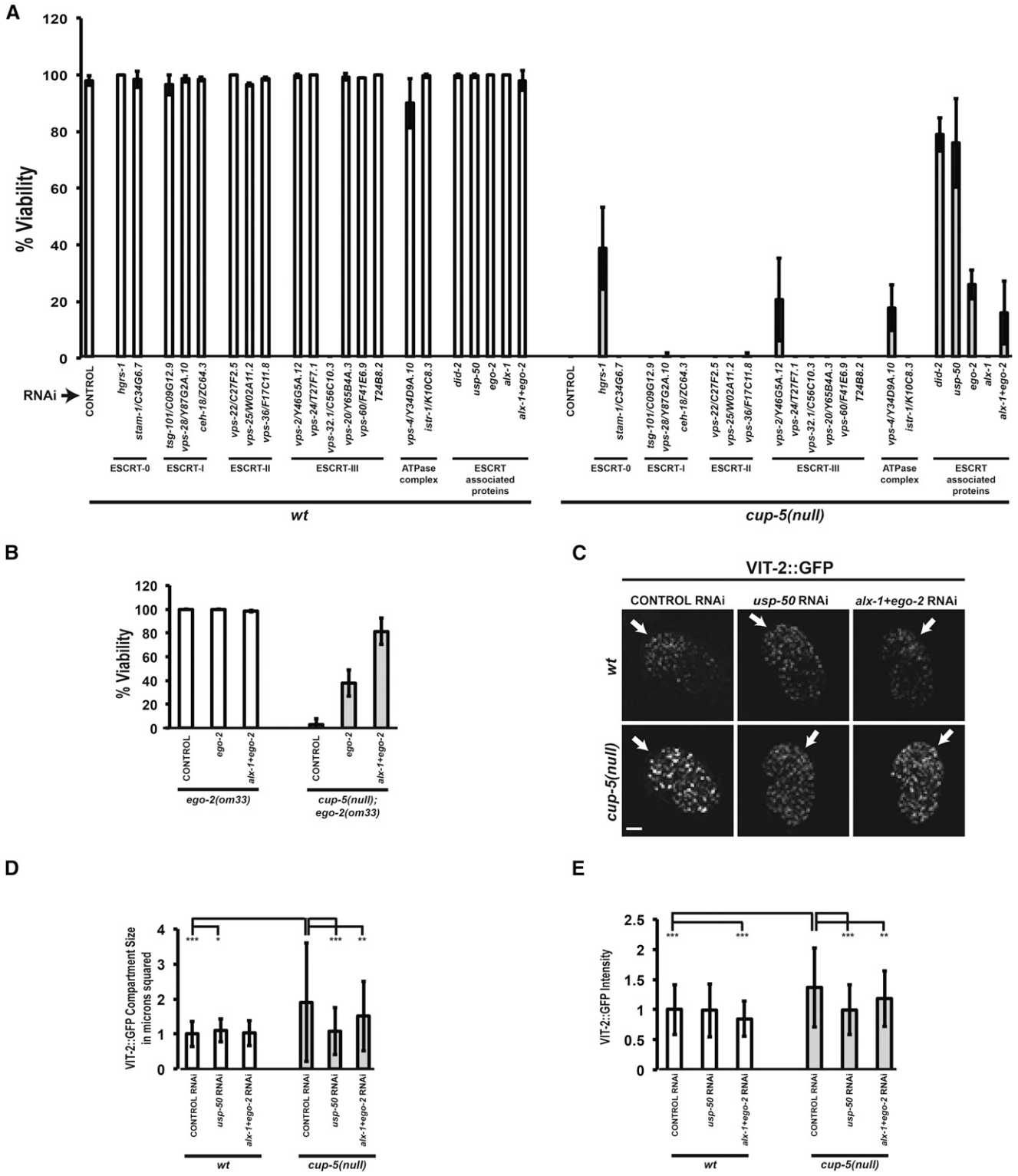

Figure 6 ESCRT RNAi suppression of *cup-5(null)* defects. (A) Percentage of viable worms laid by wild-type or *cup-5(null)* hermaphrodites after the indicated RNAi's. (B) Percentage of viable worms laid by *ego-2(om33)* or *cup-5(null)*; *ego-2(om33)* hermaphrodites after the indicated RNAi's. (C) Confocal images of comma to 1.5-fold stage embryos laid by wild-type or *cup-5(null)* hermaphrodites carrying the VIT-2::GFP transgene after the indicated RNAi's. All images were taken at the same exposure and magnification. Arrows indicate intestinal cells. Bar represents 10 μm. (D) Quantitation of surface area of VIT-2::GFP compartments in intestinal cells shown in C. (E) Quantitation of the intensity of the VIT-2::GFP compartments in intestinal cells shown in C. An asterisk indicates $P < 0.05$; two asterisks indicate $P < 0.005$; and three asterisks indicate $P < 0.0005$. Measurements were normalized to 1 in D and E using the wild-type control RNAi values.

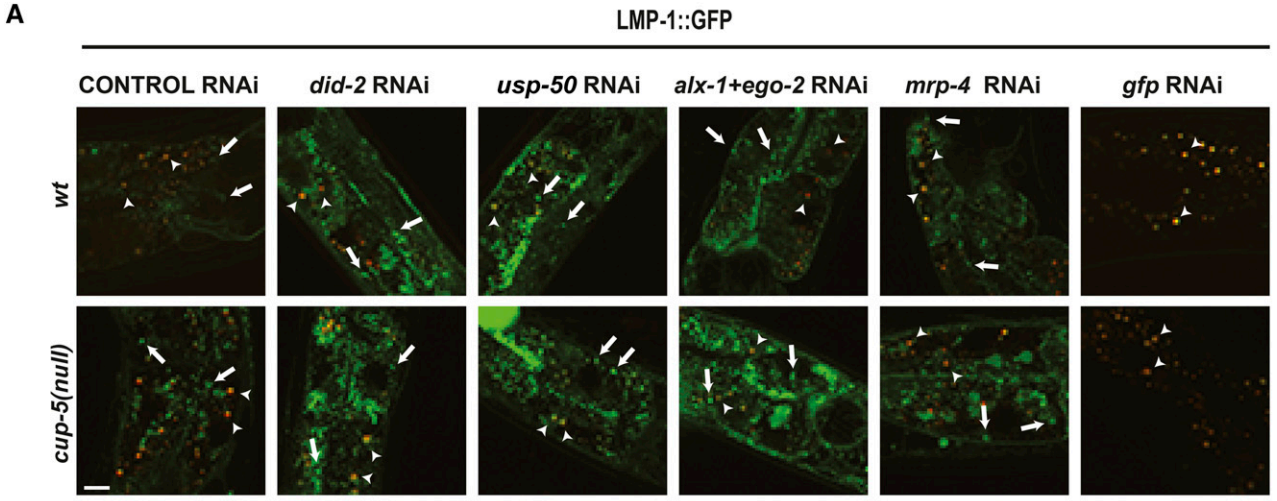

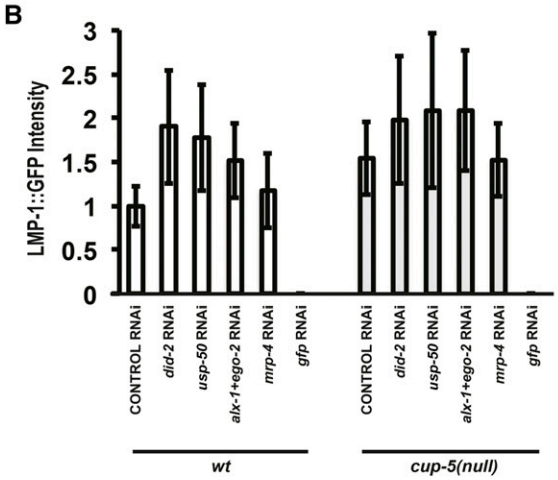

C

wt CONTROL RNAi vs *wt did-2* RNAi	2.32109E-12
wt CONTROL RNAi vs *wt usp-50* RNAi	7.16345E-11
wt CONTROL RNAi vs *wt alx-1+ego-2* RNAi	2.60833E-09
wt CONTROL RNAi vs *wt mrp-4* RNAi	0.028462298
wt CONTROL RNAi vs *cup-5(null) did-2* RNAi	5.5372E-12
wt CONTROL RNAi vs *cup-5(null) usp-50* RNAi	8.66254E-11
wt CONTROL RNAi vs *cup-5(null) alx-1+ego-2* RNAi	7.45245E-14
wt CONTROL RNAi vs *cup-5(null) mrp-4* RNAi	1.24286E-09
cup-5(null) CONTROL RNAi vs *wt* CONTROL RNAi	2.67279E-10
cup-5(null) CONTROL RNAi vs *wt did-2* RNAi	0.004204137
cup-5(null) CONTROL RNAi vs *wt usp-50* RNAi	0.049054659
cup-5(null) CONTROL RNAi vs *wt alx-1+ego-2* RNAi	0.75920455
cup-5(null) CONTROL RNAi vs *wt mrp-4* RNAi	0.000156448
cup-5(null) CONTROL RNAi vs *cup-5(null) did-2* RNAi	0.001497241
cup-5(null) CONTROL RNAi vs *cup-5(null) usp-50* RNAi	0.000762969
cup-5(null) CONTROL RNAi vs *cup-5(null) alx-1+ego-2* RNAi	0.000105969
cup-5(null) CONTROL RNAi vs *cup-5(null) mrp-4* RNAi	0.807669676
wt did-2 RNAi vs *wt usp-50* RNAi	0.375695628
wt did-2 RNAi vs *wt alx-1+ego-2* RNAi	0.002228256
wt did-2 RNAi vs *wt mrp-4* RNAi	6.38148E-08
wt did-2 RNAi vs *cup-5(null) did-2* RNAi	0.614257389
wt did-2 RNAi vs *cup-5(null) usp-50* RNAi	0.291727854
wt did-2 RNAi vs *cup-5(null) alx-1+ego-2* RNAi	0.249535435
wt did-2 RNAi vs *cup-5(null) mrp-4* RNAi	0.00247238
wt usp-50 RNAi vs *wt alx-1+ego-2* RNAi	0.028719039
wt usp-50 RNAi vs *wt mrp-4* RNAi	1.82316E-06
wt usp-50 RNAi vs *cup-5(null) did-2* RNAi	0.180047865
wt usp-50 RNAi vs *cup-5(null) usp-50* RNAi	0.072852764
wt usp-50 RNAi vs *cup-5(null) alx-1+ego-2* RNAi	0.049083953
wt usp-50 RNAi vs *cup-5(null) mrp-4* RNAi	0.03163566
wt alx-1+ego-2 RNAi vs *wt mrp-4* RNAi	0.000521951
wt alx-1+ego-2 RNAi vs *cup-5(null) did-2* RNAi	0.000805009
wt alx-1+ego-2 RNAi vs *cup-5(null) usp-50* RNAi	0.000437486
wt alx-1+ego-2 RNAi vs *cup-5(null) alx-1+ego-2* RNAi	5.61859E-05
wt alx-1+ego-2 RNAi vs *cup-5(null) mrp-4* RNAi	0.948205332
wt mrp-4 RNAi vs *cup-5(null) did-2* RNAi	4.30277E-08
wt mrp-4 RNAi vs *cup-5(null) usp-50* RNAi	9.29637E-08
wt mrp-4 RNAi vs *cup-5(null) alx-1+ego-2* RNAi	2.3046E-09
wt mrp-4 RNAi vs *cup-5(null) mrp-4* RNAi	0.000379123
cup-5(null) did-2 RNAi vs *cup-5(null) usp-50* RNAi	0.559593376
cup-5(null) did-2 RNAi vs *cup-5(null) alx-1+ego-2* RNAi	0.530067265
cup-5(null) did-2 RNAi vs *cup-5(null) mrp-4* RNAi	0.000890431
cup-5(null) usp-50 RNAi vs *cup-5(null) alx-1+ego-2* RNAi	0.991780038
cup-5(null) usp-50 RNAi vs *cup-5(null) mrp-4* RNAi	0.000480283
cup-5(null) alx-1+ego-2 RNAi vs *cup-5(null) mrp-4* RNAi	6.06373E-05

P value range	Color Key
P >0.05	
P <0.05	
P <0.005	
P <0.0005	

Figure 7 ESCRT RNAi suppression in adult intestine. (A) Confocal images of adult wild type (*wt*) and *cup-5(null)* (*zu223* allele) intestine expressing LMP-1::GFP after the indicated RNAi's. All images were taken using the same exposure and magnification. Arrows indicate LMP-1::GFP compartments. Arrowheads indicate autofluorescent gut granules. Bar, 10 μm. (B) Quantitation of the intensity of LMP-1::GFP in compartments shown in A. Measurements were normalized to 1 using the wild-type control RNAi value. (C) Table of *P* values for all pairwise tests in B.

becomes, is there a biochemical link between CUP-5 and the ESCRT-associated proteins?

Studies in other systems have uncovered a potential link between TRPML1 and ESCRT-associated proteins. Human TRPML1 binds the penta-EF-hand protein ALG2 (Vergarajauregui *et al.* 2009). In other studies, ALG2 was found to interact with Alix and HD-PTP, the human homologs of ALX-1 and EGO-2 (Missotten *et al.* 1999; Vito *et al.* 1999; Ichioka *et al.* 2007). Our future studies will probe the functionality of this potential link between the Ca^{2+} channel CUP-5, the Ca^{2+}-binding protein M04F3.4 (worm homolog of ALG2), and ALX-1/EGO-2, the yeast homolog Bro1p of which binds and activates the de-ubiquitinase Doa4p and where human HD-PTP (worm EGO-2) was found to bind UBPY (worm USP-50) as a part of EGFR's ESCRT pathway (Richter *et al.* 2007; Ali *et al.* 2013). These studies would delineate how CUP-5 regulates ESCRT-associated proteins and how these ESCRT-associated proteins are misregulated in the absence of CUP-5.

We have uncovered a novel link between CUP-5 and ESCRT-associated proteins that suggests coordinate regulation of lysosome formation and function via CUP-5 with the de-ubiquitination and intraluminal sequestration of cargo in late endosomes via ESCRT-associated proteins. This genetic link seems to be present only in certain tissues and developmental stages. Thus, CUP-5 may have functions that are unique to some tissues, which may be one of the reasons why MLIV patients and mouse models of the disease show developmental and neurological defects that are more severe than in other tissues (Altarescu *et al.* 2002; Grishchuk *et al.* 2015).

Acknowledgments

We thank Eleanor Maine (Syracuse University) for the *ego-2* cDNA construct; Patty Jansma for microscopy assistance; Bhavani Bagevalu Siddegowda for qRT-PCR assistance; and Teresa Horm for helpful discussions. This work was supported by a Microscopy Society of America grant (to J.H.) and by National Science Foundation grant 3004290 (to H.F.).

Literature Cited

Ali, N., L. Zhang, S. Taylor, A. Mironov, S. Urbe *et al.*, 2013 Recruitment of UBPY and ESCRT exchange drive HD-PTP-dependent sorting of EGFR to the MVB. Curr. Biol. 23: 453–461.

Altarescu, G., M. Sun, D. F. Moore, J. A. Smith, E. A. Wiggs *et al.*, 2002 The neurogenetics of mucolipidosis type IV. Neurology 59: 306–313.

Bach, G., 2001 Mucolipidosis type IV. Mol. Genet. Metab. 73: 197–203.

Bargal, R., N. Avidan, E. Ben-Asher, Z. Olender, M. Zeigler *et al.*, 2000 Identification of the gene causing mucolipidosis type IV. Nat. Genet. 26: 118–123.

Bassi, M. T., M. Manzoni, E. Monti, M. T. Pizzo, A. Ballabio *et al.*, 2000 Cloning of the gene encoding a novel integral membrane protein, mucolipidin, and identification of the two major founder mutations causing mucolipidosis type IV. Am. J. Hum. Genet. 67: 1110–1120.

Bauer, B. E., H. Wolfger, and K. Kuchler, 1999 Inventory and function of yeast ABC proteins: about sex, stress, pleiotropic drug and heavy metal resistance. Biochim. Biophys. Acta 1461: 217–236.

Bowers, K., J. Lottridge, S. B. Helliwell, L. M. Goldthwaite, J. P. Luzio *et al.*, 2004 Protein-protein interactions of ESCRT complexes in the yeast *Saccharomyces cerevisiae*. Traffic 5: 194–210.

Bozzato, A., S. Barlati, and G. Borsani, 2008 Gene expression profiling of mucolipidosis type IV fibroblasts reveals deregulation of genes with relevant functions in lysosome physiology. Biochim. Biophys. Acta 1782: 250–258.

Brenner, S., 1974 The genetics of *Caenorhabditis elegans*. Genetics 77: 71–94.

Campbell, E. M., and H. Fares, 2010 Roles of CUP-5, the *Caenorhabditis elegans* orthologue of human TRPML1, in lysosome and gut granule biogenesis. BMC Cell Biol. 11: 40.

Colletti, G. A., M. T. Miedel, J. Quinn, N. Andharia, O. A. Weisz *et al.*, 2012 Loss of lysosomal ion channel transient receptor potential channel mucolipin-1 (TRPML1) leads to cathepsin B-dependent apoptosis. J. Biol. Chem. 287: 8082–8091.

Dean, M., Y. Hamon, and G. Chimini, 2001 The human ATP-binding cassette (ABC) transporter superfamily. J. Lipid Res. 42: 1007–1017.

Dong, X. P., X. Cheng, E. Mills, M. Delling, F. Wang *et al.*, 2008 The type IV mucolipidosis-associated protein TRPML1 is an endolysosomal iron release channel. Nature 455: 992–996.

Fares, H., and I. Greenwald, 2001a Genetic analysis of endocytosis in *Caenorhabditis elegans*: coelomocyte uptake defective mutants. Genetics 159: 133–145.

Fares, H., and I. Greenwald, 2001b Regulation of endocytosis by CUP-5, the *Caenorhabditis elegans* mucolipin-1 homolog. Nat. Genet. 28: 64–68.

Fukushige, T., M. G. Hawkins, and J. D. McGhee, 1998 The GATA-factor *elt-2* is essential for formation of the *Caenorhabditis elegans* intestine. Dev. Biol. 198: 286–302.

Goujon, M., H. McWilliam, W. Z. Li, F. Valentin, S. Squizzato *et al.*, 2010 A new bioinformatics analysis tools framework at EMBL-EBI. Nucleic Acids Res. 38: W695–W699.

Graham, P. L., and J. Kimble, 1993 The *mog-1* gene is required for the switch from spermatogenesis to oogenesis in *Caenorhabditis elegans*. Genetics 133: 919–931.

Grant, B., and D. Hirsh, 1999 Receptor-mediated endocytosis in the *Caenorhabditis elegans* oocyte. Mol. Biol. Cell 10: 4311–4326.

Grishchuk, Y., K. A. Pena, J. Coblentz, V. E. King, D. M. Humphrey *et al.*, 2015 Impaired myelination and reduced brain ferric iron in the mouse model of mucolipidosis IV. Dis. Model. Mech. 8: 1591–160.

Hadwiger, G., S. Dour, S. Arur, P. Fox, and M. L. Nonet, 2010 A monoclonal antibody toolkit for C. elegans. PLoS One 5: e10161.

Henne, W. M., N. J. Buchkovich, and S. D. Emr, 2011 The ESCRT pathway. Dev. Cell 21: 77–91.

Hersh, B. M., E. Hartwieg, and H. R. Horvitz, 2002 The *Caenorhabditis elegans* mucolipin-like gene *cup-5* is essential for viability and regulates lysosomes in multiple cell types. Proc. Natl. Acad. Sci. USA 99: 4355–4360.

Ichioka, F., E. Takaya, H. Suzuki, S. Kajigaya, V. L. Buchman *et al.*, 2007 HD-PTP and Alix share some membrane-traffic related proteins that interact with their Bro1 domains or proline-rich regions. Arch. Biochem. Biophys. 457: 142–149.

Kamath, R. S., and J. Ahringer, 2003 Genome-wide RNAi screening in *Caenorhabditis elegans*. Methods 30: 313–321.

Katzmann, D. J., M. Babst, and S. D. Emr, 2001 Ubiquitin-dependent sorting into the multivesicular body pathway requires the function of a conserved endosomal protein sorting complex, ESCRT-I. Cell 106: 145–155.

Kostich, M., A. Fire, and D. M. Fambrough, 2000 Identification and molecular-genetic characterization of a LAMP/CD68-like protein from *Caenorhabditis elegans*. J. Cell Sci. 113(Pt 14): 2595–2606.

Lapierre, L. R., C. D. De Magalhaes Filho, P. R. McQuary, C. C. Chu, O. Visvikis *et al.*, 2013 The TFEB orthologue HLH-30 regulates autophagy and modulates longevity in *Caenorhabditis elegans*. Nat. Commun. 4: 2267.

LaPlante, J. M., J. Falardeau, M. Sun, M. Kanazirska, E. M. Brown *et al.*, 2002 Identification and characterization of the single channel function of human mucolipin-1 implicated in mucolipidosis type IV, a disorder affecting the lysosomal pathway. FEBS Lett. 532: 183–187.

Liu, Y., and E. M. Maine, 2007 The Bro1-domain protein, EGO-2, promotes Notch signaling in *Caenorhabditis elegans*. Genetics 176: 2265–2277.

Mahul-Mellier, A. L., F. J. Hemming, B. Blot, S. Fraboulet, and R. Sadoul, 2006 Alix, making a link between apoptosis-linked gene-2, the endosomal sorting complexes required for transport, and neuronal death in vivo. J. Neurosci. 26: 542–549.

Medina, D. L., S. Di Paola, I. Peluso, A. Armani, D. De Stefani *et al.*, 2015 Lysosomal calcium signalling regulates autophagy through calcineurin and TFEB. Nat. Cell Biol. 17: 288–299.

Miller, A., J. Schafer, C. Upchurch, E. Spooner, J. Huynh *et al.*, 2015 Mucolipidosis type IV protein TRPML1-dependent lysosome formation. Traffic 16: 284–297.

Missotten, M., A. Nichols, K. Rieger, and R. Sadoul, 1999 Alix, a novel mouse protein undergoing calcium-dependent interaction with the apoptosis-linked-gene 2 (ALG-2) protein. Cell Death Differ. 6: 124–129.

Moerman, D. G., and R. J. Barstead, 2008 Towards a mutation in every gene in *Caenorhabditis elegans*. Brief. Funct. Genomics Proteomics 7: 195–204.

Nickerson, D. P., M. West, and G. Odorizzi, 2006 Did2 coordinates Vps4-mediated dissociation of ESCRT-III from endosomes. J. Cell Biol. 175: 715–720.

Pfaffl, M. W., 2001 A new mathematical model for relative quantification in real-time RT-PCR. Nucleic Acids Res. 29: e45.

Praitis, V., E. Casey, D. Collar, and J. Austin, 2001 Creation of low-copy integrated transgenic lines in *Caenorhabditis elegans*. Genetics 157: 1217–1226.

Qiao, L., J. L. Lissemore, P. Shu, A. Smardon, M. B. Gelber *et al.*, 1995 Enhancers of glp-1, a gene required for cell-signaling in *Caenorhabditis elegans*, define a set of genes required for germline development. Genetics 141: 551–569.

Raychowdhury, M. K., S. Gonzalez-Perrett, N. Montalbetti, G. A. Timpanaro, B. Chasan *et al.*, 2004 Molecular pathophysiology of mucolipidosis type IV: pH dysregulation of the mucolipin-1 cation channel. Hum. Mol. Genet. 13: 617–627.

Reggiori, F., and H. R. Pelham, 2001 Sorting of proteins into multivesicular bodies: ubiquitin-dependent and -independent targeting. EMBO J. 20: 5176–5186.

Reid, E., J. Connell, T. L. Edwards, S. Duley, S. E. Brown *et al.*, 2005 The hereditary spastic paraplegia protein spastin interacts with the ESCRT-III complex-associated endosomal protein CHMP1B. Hum. Mol. Genet. 14: 19–38.

Richter, C., M. West, and G. Odorizzi, 2007 Dual mechanisms specify Doa4-mediated deubiquitination at multivesicular bodies. EMBO J. 26: 2454–2464.

Row, P. E., H. Liu, S. Hayes, R. Welchman, P. Charalabous *et al.*, 2007 The MIT domain of UBPY constitutes a CHMP binding and endosomal localization signal required for efficient epidermal growth factor receptor degradation. J. Biol. Chem. 282: 30929–30937.

Rual, J. F., J. Ceron, J. Koreth, T. Hao, A. S. Nicot *et al.*, 2004 Toward improving *Caenorhabditis elegans* phenome mapping with an ORFeome-based RNAi library. Genome Res. 14: 2162–2168.

Sambrook, J., and D. W. Russell, 2001 *Molecular Cloning: A Laboratory Manual*. Cold Spring Harbor Laboratory Press, Cold Spring Harbor, NY.

Sardiello, M., M. Palmieri, A. di Ronza, D. L. Medina, M. Valenza *et al.*, 2009 A gene network regulating lysosomal biogenesis and function. Science 325: 473–477.

Schaheen, L., H. Dang, and H. Fares, 2006a Basis of lethality in *C. elegans* lacking CUP-5, the mucolipidosis type IV orthologue. Dev. Biol. 293: 382–391.

Schaheen, L., G. Patton, and H. Fares, 2006b Suppression of the *cup-5* mucolipidosis type IV-related lysosomal dysfunction by the inactivation of an ABC transporter in *C. elegans*. Development 133: 3939–3948.

Schneider, C. A., W. S. Rasband, and K. W. Eliceiri, 2012 NIH Image to ImageJ: 25 years of image analysis. Nat. Methods 9: 671–675.

Sheps, J. A., S. Ralph, Z. Zhao, D. L. Baillie, and V. Ling, 2004 The ABC transporter gene family of *Caenorhabditis elegans* has implications for the evolutionary dynamics of multidrug resistance in eukaryotes. Genome Biol. 5: R15.

Sievers, F., A. Wilm, D. Dineen, T. J. Gibson, K. Karplus *et al.*, 2011 Fast, scalable generation of high-quality protein multiple sequence alignments using Clustal Omega. Mol. Syst. Biol. 7: 539.

Sun, M., E. Goldin, S. Stahl, J. L. Falardeau, J. C. Kennedy *et al.*, 2000 Mucolipidosis type IV is caused by mutations in a gene encoding a novel transient receptor potential channel. Hum. Mol. Genet. 9: 2471–2478.

Timmons, L., and A. Fire, 1998 Specific interference by ingested dsRNA. Nature 395: 854.

Treusch, S., S. Knuth, S. A. Slaugenhaupt, E. Goldin, B. D. Grant *et al.*, 2004 *Caenorhabditis elegans* functional orthologue of human protein h-mucolipin-1 is required for lysosome biogenesis. Proc. Natl. Acad. Sci. USA 101: 4483–4488.

Vergarajauregui, S., J. A. Martina, and R. Puertollano, 2009 Identification of the penta-EF-hand protein ALG-2 as a Ca^{2+}-dependent interactor of mucolipin-1. J. Biol. Chem. 284: 36357–36366.

Vito, P., L. Pellegrini, C. Guiet, and L. D'Adamio, 1999 Cloning of AIP1, a novel protein that associates with the apoptosis-linked gene ALG-2 in a Ca^{2+}-dependent reaction. J. Biol. Chem. 274: 1533–1540.

Communicating editor: B. Goldstein

GENETICS

Supporting Information
www.genetics.org/lookup/suppl/doi:10.1534/genetics.115.182485/-/DC1

ESCRT-Dependent Cell Death in a *Caenorhabditis elegans* Model of the Lysosomal Storage Disorder Mucolipidosis Type IV

Julie M. Huynh, Hope Dang, Isabel A. Munoz-Tucker, Marvin O'Ketch, Ian T. Liu, Savannah Perno, Natasha Bhuyan, Allison Crain, Ivan Borbon, and Hanna Fares

DOI: 10.1534/genetics.115.182485

A

```
C.e. DID-2          MGAGESSMALEKHLFDLKFAAKQLEKNAQRCEKDEKVEKQKLTAAIKKGNKEVAQVHAEN  60
S.c. Did2p          -MSRNSAAGLENTLFQLKFTSKQLQKQANKASKEEKQETNKLKRALN-ENEDISRIYASN  58
H.s. CHMP1b         ------MSNMEKHLFNLKFAAKELSNSAKKCDKEEKAEKAKIKKAIQKGNMEVARIHAEN  54

C.e. DID-2          AIRKKNEAVNYIKMAARIDAVAARVQTAATQKRVTASMSGVVKAMESAMKSMNLEKVQQL  120
S.c. Did2p          AIRKKNERLQLLKLASRVDSVASRVQTAVTMRQVSASMGQVCKGMDKALQNMNLQQITMI  118
H.s. CHMP1b         AIRQKNQAVNFLRMSARVDAVAARVQTAVTMGKVTKSMAGVVKSMDATLKTMNLEKISAL  114

C.e. DID-2          MDRFERDFEDLDVHTKTMEKTMDGTTVLNAPKSQVDALIAEAADKAGLELNQELPSNVPT  180
S.c. Did2p          MDKFEQQFEDLDTSVNVYEDMGVNSDAMLVDNDKVDELMSKVADENGMELKQSAKLDNVP  178
H.s. CHMP1b         MDKFEHQFETLDVQTQQMEDTMSSTTTLITPQNQVDMLIQEMADEAGLDLNMELPQGQTG  174

C.e. DID-2          APPTGTQ--AVSEDKILERLAALRNM                                  205
S.c. Did2p          EIKAKEVNVDDEKEDKLAQRLRALRG                                  204
H.s. CHMP1b         SVGTSVA---SAEQDELSQRLARLRDQV                                199
```

B

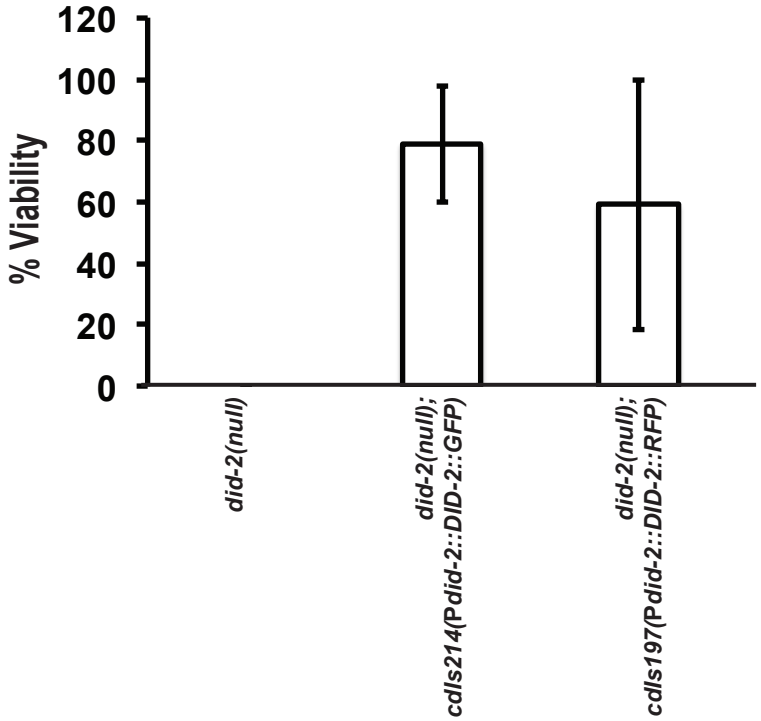

Figure S1. Worm DID-2 sequence, similarity to yeast and human proteins, and DID-2::GFP/TagRFP functionality. (A) Shown is the amino acid sequence alignment of DID-2 (*C. elegans*), Did2p (*S. cerevisiae*), and CHMP1b (*H. sapiens*). Identical amino acids are shaded in black while similar amino acids are shaded in grey. Amino acids considered similar were I/L/V, S/T, D/E, and K/R. (B) Percent of laid embryos that hatched and grew to adults from *did-2(ok3325)* (null allele) hermaphrodites carrying a DID-2::GFP or DID-2::Tag RFP transgene. This partial rescue is expected because transgenes are not expressed in the germline; therefore, they cannot rescue early defects in embryogenesis.

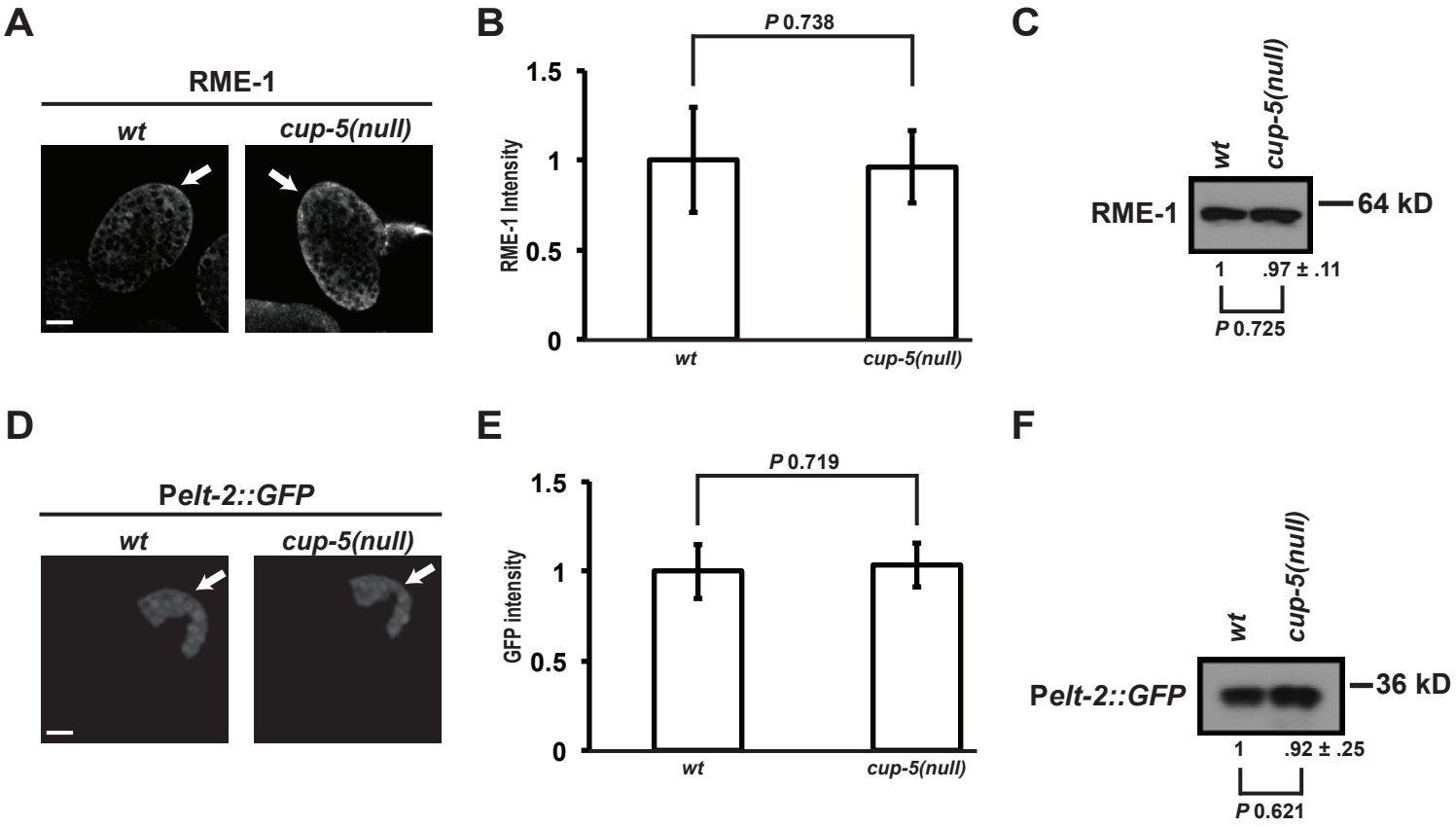

Figure S2. RME-1 levels and P*elt-2* activity in wild type and *cup-5(null).* (A) Confocal images of "1.5-fold" stage embryos laid by wild type (*wt*) or *cup-5(null)* (*zu223* allele) hermaphrodites immunostained for RME-1. All images were taken at the same exposure and magnitification. Arrows indicate intestinal cell staining. (B) Quantitation of the intensity of RME-1 in intestinal cells shown in A. (C) Western blot showing RME-1 levels in embryos laid by wild type or *cup-5(null)* hermaphrodites. Equal amount of total protein levels were loaded. The numbers are the average of three independent trials. (D) Confocal images of "1.5-fold" stage embryos laid by wild type or *cup-5(null)* hermaphrodites expressing GFP under the control of the *elt-2* promoter. All images were taken at the same exposure and magnification. Arrows indicate intestinal cell staining. (E) Quantitation of the intensity of GFP in intestinal cells shown in D. (F) Western blot showing GFP levels in embryos laid by wild type or *cup-5(null)* hermaphrodites. Equal amount of total protein levels were loaded. The numbers are the average of three independent trials. The indicated *P* values are from Student's *t*-test. Scale bars represent 10 μm in all images.

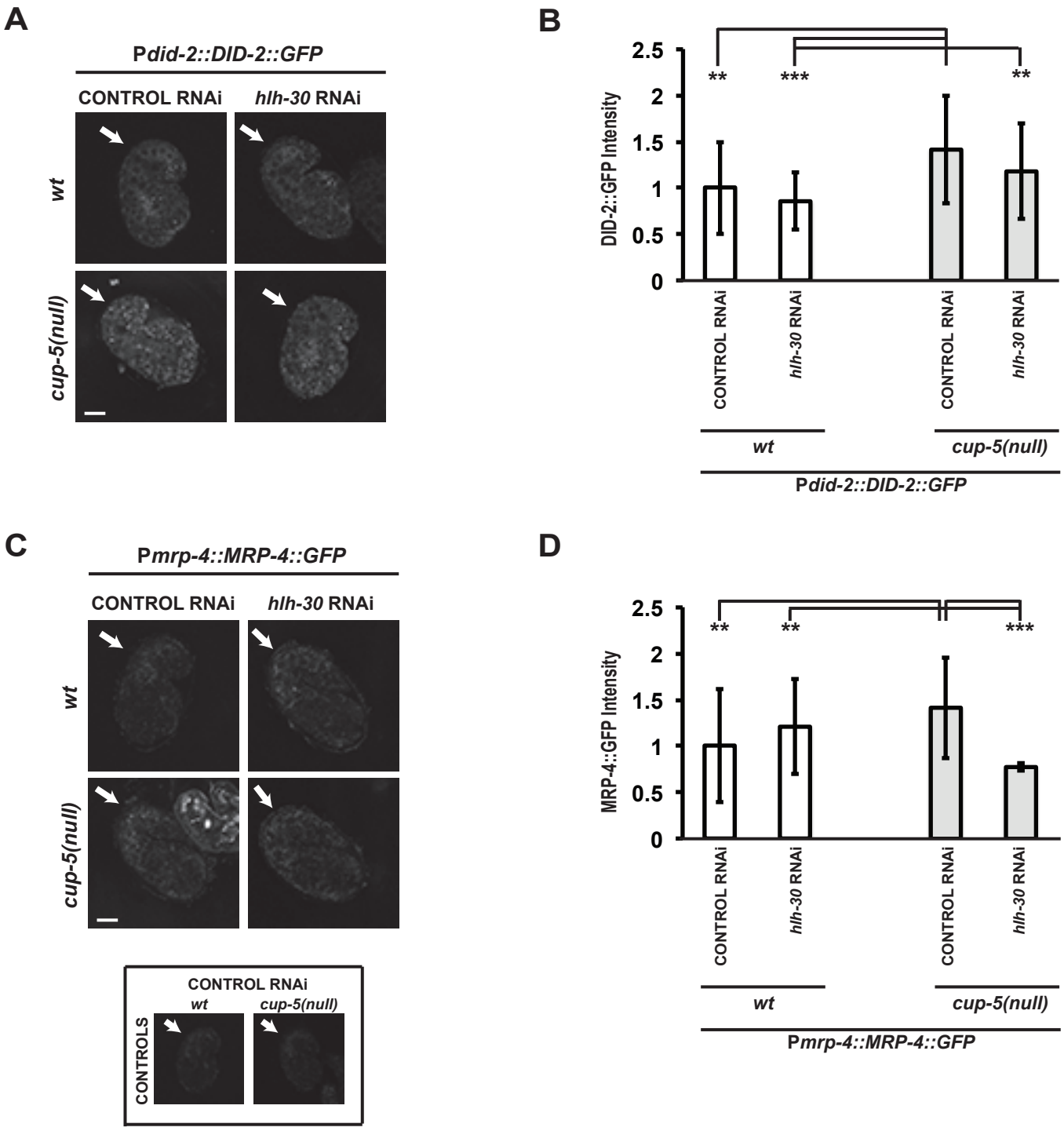

Figure S3. Effect of TFEB homologue HLH-30 RNAi on MRP-4::GFP and DID-2::GFP.
(A) Confocal images of "1.5-fold" stage embryos laid by P*did-2::DID-2::GFP* wild type or *cup-5(zu223)* hermaphrodites after the indicated RNAis. All images were taken using the same exposure and magnification. Arrows indicate intestinal cells. Under these microscopy conditions, embryos lacking this transgene showed no background fluorescence. (B) Quantitation of DID-2::GFP levels in intestinal cells shown in A. (C) Confocal images of "1.5-fold" stage embryos laid by P*mrp-4::MRP-4::GFP* wild type or *cup-5(zu223)* hermaphrodites after the indicated RNAis. All images were taken using the same exposure and magnification. Arrows indicate intestinal cells. (D) Quantitation of MRP-4::GFP levels in intestinal cells shown in C. Background immunofluorescence values from wild type and *cup-5(zu223)* embryos not carrying the MRP-4::GFP transgene were subtracted. Two asterisks indicates $P<0.005$. Three asterisks indicates $P<0.0005$. Measurements were normalized to 1 in B and D using the wild type control RNAi values. Scale bars represent 10 μm in all images.

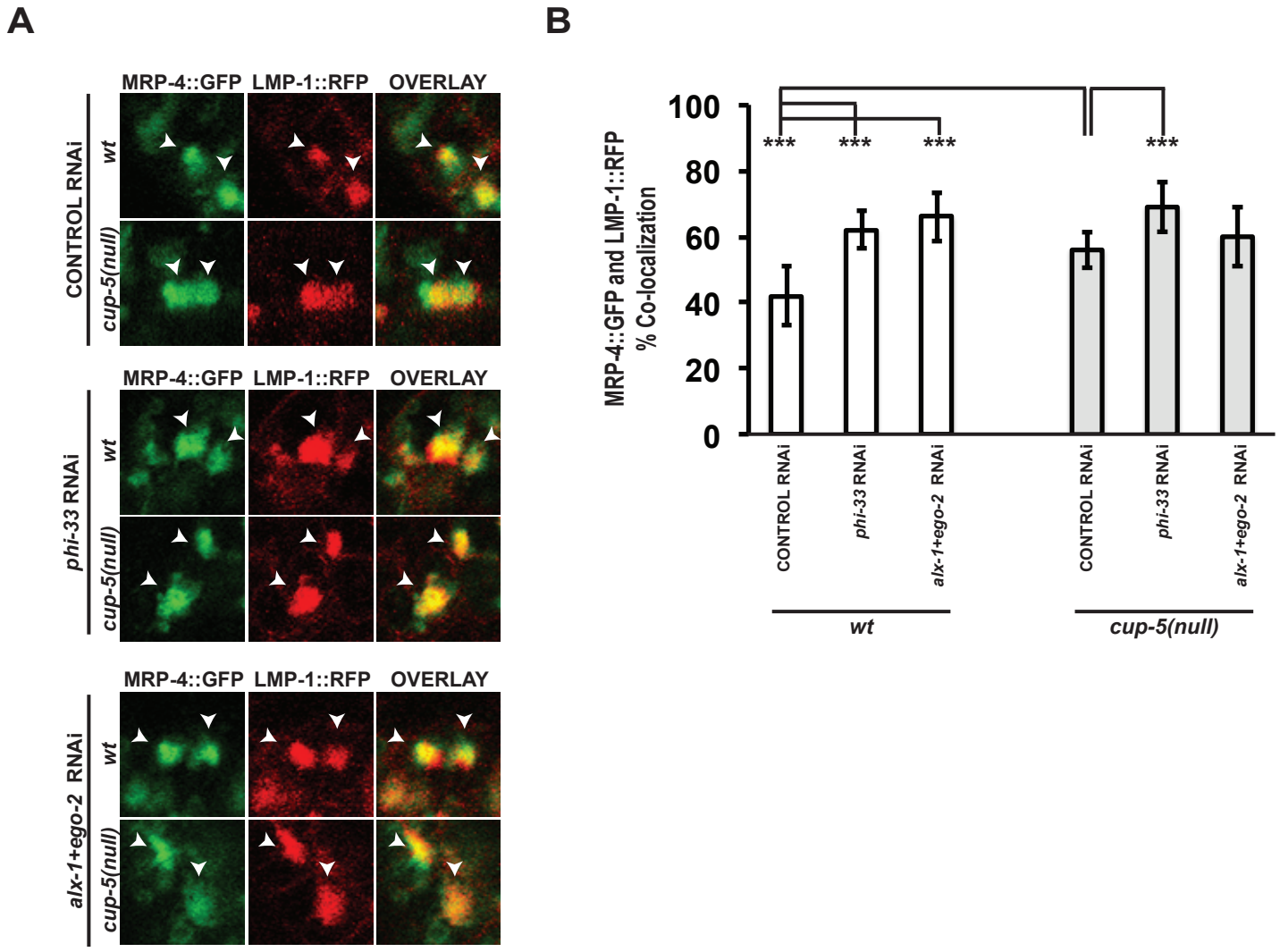

Figure S4. MRP-4::GFP protein localization with LMP-1::RFP in wild type and *cup-5(null)* after ESCRT-associated protein RNAi. (A) Confocal images of "1.5-fold" stage embryos laid by wild type or *cup-5(null)* hermaphrodites expressing MRP-4::GFP and LMP-1::RFP after the indicated RNAis. Only the magnified images are shown. Arrowheads indicate co-localization. (B) Quantitation of MRP-4::GFP and LMP-1::RFP percent co-localization in intestinal cells shown in A. Three asterisks indicates $P<0.0005$.

A

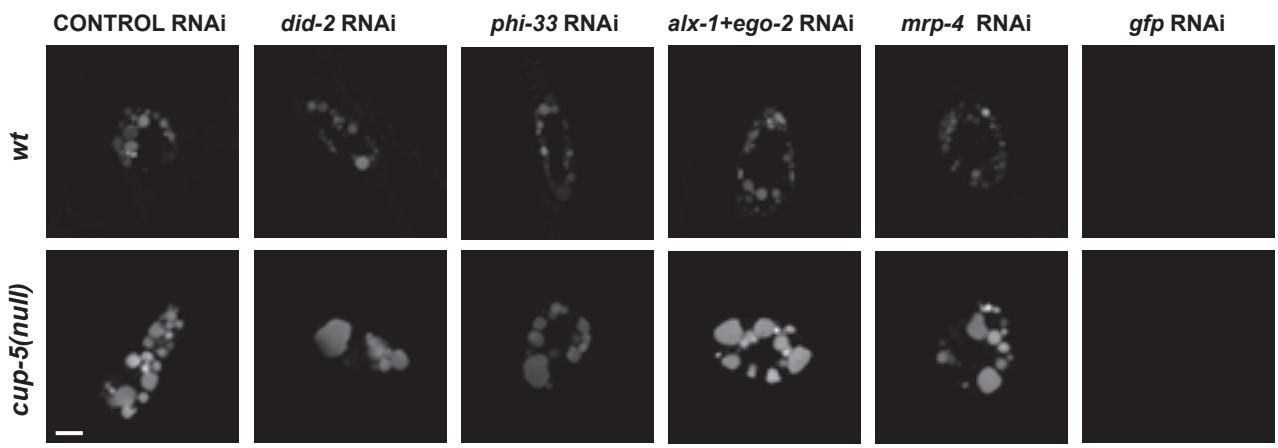

B

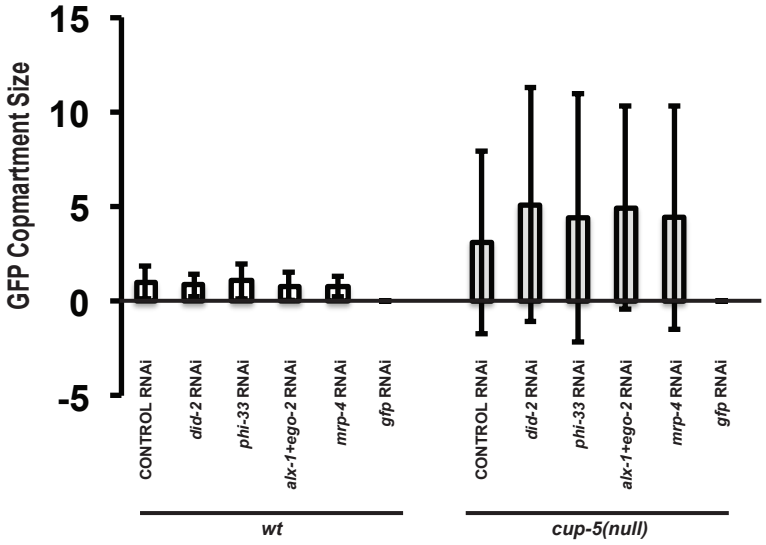

C

wt CONTROL RNAi vs *wt did-2* RNAi	0.201931013
wt CONTROL RNAi vs *wt phi-33* RNAi	0.719503989
wt CONTROL RNAi vs *wt alx-1+ego-2* RNAi	0.068370574
wt CONTROL RNAi vs *wt mrp-4* RNAi	0.023268117
wt CONTROL RNAi vs *cup-5(null) did-2* RNAi	1.78016E-09
wt CONTROL RNAi vs *cup-5(null) phi-33* RNAi	1.38738E-06
wt CONTROL RNAi vs *cup-5(null) alx-1+ego-2* RNAi	8.97972E-11
wt CONTROL RNAi vs *cup-5(null) mrp-4* RNA	1.05848E-07
cup-5(null) CONTROL RNAi vs *wt* CONTROL RNAi	4.7432E-05
cup-5(null) CONTROL RNAi vs *wt did-2* RNAi	0.000297335
cup-5(null) CONTROL RNAi vs *wt phi-33* RNAi	0.000119322
cup-5(null) CONTROL RNAi vs *wt alx-1+ego-2* RNAi	2.20612E-05
cup-5(null) CONTROL RNAi vs *wt mrp-4* RNAi	5.7372E-07
cup-5(null) CONTROL RNAi vs *cup-5(null) did-2* RNAi	0.029885336
cup-5(null) CONTROL RNAi vs *cup-5(null) phi-33* RNAi	0.153936609
cup-5(null) CONTROL RNAi vs *cup-5(null) alx-1+ego-2* RNAi	0.04108011
cup-5(null) CONTROL RNAi vs *cup-5(null) mrp-4* RNAi	0.145729792
wt did-2 RNAi vs *wt phi-33* RNAi	0.122565445
wt did-2 RNAi vs *wt alx-1+ego-2* RNAi	0.588889313
wt did-2 RNAi vs *wt mrp-4* RNAi	0.476149831
wt did-2 RNAi vs *cup-5(null) did-2* RNAi	2.32282E-07
wt did-2 RNAi vs *cup-5(null) phi-33* RNAi	3.12107E-05
wt did-2 RNAi vs *cup-5(null) alx-1+ego-2* RNAi	2.07966E-08
wt did-2 RNAi vs *cup-5(null) mrp-4* RNAi	4.17725E-06
wt phi-33 RNAi vs *wt alx-1+ego-2* RNAi	0.037583954
wt phi-33 RNAi vs *wt mrp-4* RNAi	0.009959847
wt phi-33 RNAi vs *cup-5(null) did-2* RNAi	8.29314E-09
wt phi-33 RNAi vs *cup-5(null) phi-33* RNAi	4.03117E-06
wt phi-33 RNAi vs *cup-5(null) alx-1+ego-2* RNAi	5.4814E-10
wt phi-33 RNAi vs *cup-5(null) mrp-4* RNAi	3.84049E-07
wt alx-1+ego-2 RNAi vs *wt mrp-4* RNAi	0.987344613
wt alx-1+ego-2 RNAi vs *cup-5(null) did-2* RNAi	2.25755E-09
wt alx-1+ego-2 RNAi vs *cup-5(null) phi-33* RNAi	1.279E-06
wt alx-1+ego-2 RNAi vs *cup-5(null) alx-1+ego-2* RNAi	1.03146E-10
wt alx-1+ego-2 RNAi vs *cup-5(null) mrp-4* RNAi	9.46938E-08
wt mrp-4 RNAi vs *cup-5(null) did-2* RNAi	2.26542E-12
wt mrp-4 RNAi vs *cup-5(null) phi-33* RNAi	1.23225E-08
wt mrp-4 RNAi vs *cup-5(null) alx-1+ego-2* RNAi	3.22415E-14
wt mrp-4 RNAi vs *cup-5(null) mrp-4* RNAi	3.40492E-10
cup-5(null) did-2 RNAi vs *cup-5(null) phi-33* RNAi	0.541979766
cup-5(null) did-2 RNAi vs *cup-5(null) alx-1+ego-2* RNAi	0.881221984
cup-5(null) did-2 RNAi vs *cup-5(null) mrp-4* RNAi	0.563509272
cup-5(null) phi-33 RNAi vs *cup-5(null) alx-1+ego-2* RNAi	0.6434208
cup-5(null) phi-33 RNAi vs *cup-5(null) mrp-4* RNAi	0.980159277
cup-5(null) alx-1+ego-2 RNAi vs *cup-5(null) mrp-4* RNAi	0.657144657

P value range	Color Key
P >0.05	
P <0.05	
P <0.0005	

Figure S5. ESCRT RNAi suppression in adult coelomocytes. (A) Confocal images of endocytosed GFP in adult wild type (*wt*) and *cup-5(null)* (*zu223 allele*) coelomocytes after the indicated RNAis. Scale bar represents 5 μm. (B) Quantitation of the GFP compartment sizes shown in A. Measurements were normalized to 1 using the wild type control RNAi value. (C) Table of *P* values for all pairwise tests in B.